

CONTAMINANTS REMOVAL FROM NATURAL GAS
USING DUAL HOLLOW FIBER MEMBRANE CONTACTORS

JINGJING CAI



**CONTAMINANTS REMOVAL FROM NATURAL GAS USING
DUAL HOLLOW FIBER MEMBRANE CONTACTORS**

by

Jingjing Cai

A thesis submitted to the
School of Graduate Studies
in partial fulfillment of the
requirements for the degree of

Master of Engineering

Faculty of Engineering and Applied Science

Memorial University of Newfoundland

December 2009

St. John's

Newfoundland

Abstract

Hollow fiber membrane contactors are advantageous in natural gas processing where the required equipment foot-print is small. This is due to the larger available gas-liquid contactor area, a greater mass transfer coefficient and higher removal efficiencies. Traditionally, the hollow fiber membrane contactors used for gas-liquid contacting were designed to have separate absorption and regeneration system, which may not be practical for offshore application due to limited space. A dual membrane concept is proposed in this work which combines the contactor and stripper into one unit operation. In this design, the gas flows through the porous membranes immersed in a solvent; the solvent strips the gas of the contaminant. Nonporous membranes with a sweep gas flowing or under low pressure in the same shell, partially regenerate the solvent by stripping the contaminant out. In addition, baffles were introduced into the dual membrane module to increase the mass transfer by minimizing shell-side bypass and increasing liquid velocity. The proposed modules and an ordinary single hollow fiber membrane contactor were modeled using partial differential equations based on a single-component absorption scheme. A numerical model based on mass balance was developed to predict the performance of the dual contactor modules and also concentration change in both gas and liquid phase in the modules.

Simulation results show that the nonporous membranes in the dual hollow fiber membrane contactor can partially regenerate the solvent during the absorption and

result in a better gas removal efficiency than the ordinary module. In addition, the baffles were proved to increase the mass transfer by minimizing shell-side bypass and increasing liquid velocity. The predictions of the developed numerical model were found to be in good agreement with the previous experimental results presented by Dindore *et al.*(2005).

Acknowledgements

I would like to express my sincere gratitude to my supervisors Dr. Kelly Hawboldt and Dr. Majid A. Abdi and for their enthusiastic guidance, supervision and encouragement during the period of my study. Their concerns and supports make the experience of working with them has been more than rewarding.

Special thanks go to the School of Graduate Studies at Memorial University of Newfoundland and the Faculty of Engineering and Applied Science for their financial support.

I would also give my appreciation to Professors in Engineering for courses they offered and to my fellow graduate students, for friendship and pleasant memory we shared in the last two years.

At last, I would like to thank my parents for their support; I will not be here without their love and encouragement.

Table of Contents

Abstract.....	i
Acknowledgements	iii
Table of Contents	iv
List of Figures	vi
List of Tables.....	viii
Nomenclature.....	ix
Chapter 1 Introduction.....	1
1.1 Background.....	1
1.2 Scope of study.....	2
1.3 Objectives of study.....	4
1.4 Thesis outline.....	5
Chapter 2 Introduction to Hollow Fibre Membrane Contactors	7
2.1 Introduction to Membrane Gas Absorption Technology	7
2.1.1 Porous and Nonporous Membranes.....	7
2.2 Transport in Membranes	8
2.2.1 Transport in Porous Membranes.....	9
2.2.2 Transport in Non-Porous Membranes.....	11
2.2.3 Membrane Modules	12
2.2 Hollow Fiber Membrane Contactors (HFMC)	14
2.2.1 Flow Direction in Hollow Fiber Membrane Contactors.....	15
2.2.2 Wetted and Non-wetted Mode.....	17
2.2.3 Overall Mass Transfer.....	18
2.3 Natural Gas Processing with Membranes	19
Chapter 3 Mathematical Model Development	22
3.1 Assumptions for Model Development.....	23
3.2 Mass Transfer Fundamentals.....	23
3.2.1 Overall Mass transfer in the liquid phase	24
3.2.2 Gas phase mass balance within porous membranes	25
3.2.3 Gas phase mass balance within nonporous membranes	26
3.3 Module Development	28
3.3.1 Module I.....	28
3.3.2 Module II.....	31
3.3.3 Ordinary Hollow Fiber Contactor.....	32
3.4 Computational Fluid Dynamics (CFD).....	33
Chapter 4 Solutions to Model Equations.....	35

4.1 Numerical Solution	35
4.2 Model Validation.....	37
4.2.1 Mass Transfer Coefficient on Fiber Side	39
4.2.2 Comparison of Model Predictions and Experiment Measurements	41
4.3 Dual Membrane Module I	43
4.3.1 Mass Transfer correlation on shell side	44
4.3.2 Absorption Performance under Constant Flow Velocity	45
4.4 Dual Membrane Module II.....	49
4.4.1 Absorption Performance under Constant Flow velocity.....	50
4.5 Ordinary Membrane Contactor.....	51
4.6 Comparison of Module Performances.....	54
4.7 Fluid Dynamics in Module II	57
Chapter 5 Analysis of Model Parameters	60
5.1 Module Length.....	60
5.2 Solvent Flow Rate.....	61
5.3 Gas Flow Rate.....	63
5.4 Pressure on the Permeate Side.....	64
5.5 The Henry's Constant.....	65
5.6 Diffusion coefficient	66
5.7 Number of Baffles.....	67
5.8 Permeability of nonporous fibres.....	68
Chapter 6 Conclusions	70
6.1 Summary.....	70
6.2 Conclusions	71
6.3 Follow-up work.....	72
References	74
Appendix A	77
A.1 Grid Generation.....	77
A.2 Contours of liquid velocity magnitude in shell side of Module II.....	78

List of Figures

Figure 1.1 Proposed dual membrane contactor: Module I.....	4
Figure 1.2 Proposed dual membrane contactor with baffles: Module II	4
Figure 2.1 Schematic drawings of Poisseuille and Knudsen flows.....	10
Figure 2.2 Schematic drawing of a plate-and-frame module	13
Figure 2.3 Schematic drawing of a spiral-wound module	13
Figure 2.4 Schematic drawing of a HFMC module.....	14
Figure 2.5 Surface areas to volume ratios of various membrane module configurations	15
Figure 2.6 (a) Parallel-flow hollow fiber module; (b) cross-flow hollow fiber module.....	16
Figure 2.7 Wetted and Non-wetted mode of membrane-based gas-liquid contacting	17
Figure 2.8 Mass transfer regions in a membrane contactor	19
Figure 3.1 Cross section and modeling parameters in cross flow membrane contactor	24
Figure 3.2 Schematic structure of dual HFMC: Module I	28
Figure 3.3 Schematic structure of dual HFMC: Module II.....	31
Figure 3.4 Schematic structure of Ordinary single membrane HFMC.....	32
Figure 4.1 Cross flow membrane Module.....	38
Figure 4.2 Mass transfer coefficient in Polypropylene hollow fiber membrane contactor	41
Figure 4.3 CO ₂ concentration profile at gas outlet under different liquid flow rate for constant inlet gas flow rate of $2.21 \times 10^{-4} \text{ m}^3/\text{s}$ and inlet gas concentration of 14.62 mol/m^3	42

Figure 4.4 CO ₂ concentration profile at liquid outlet under different liquid flow rate for constant inlet gas flow rate of $2.21 \times 10^{-4} \text{ m}^3/\text{s}$ and inlet gas concentration of 14.62 mol/m^3	43
Figure 4.5 Fiber-side concentration profile of 39.33 mol/m^3 CO ₂ absorption in Module I for constant inlet gas flow rate of $2.66 \times 10^{-4} \text{ m}^3/\text{s}$ and liquid flow rate of $1.74 \times 10^{-4} \text{ m}^3/\text{s}$	46
Figure 4.6 Fiber side concentration profile of 39.33 mol/m^3 CO ₂ in Module I for constant inlet gas flow rate of $2.66 \times 10^{-4} \text{ m}^3/\text{s}$ and liquid flow rate of $1.74 \times 10^{-4} \text{ m}^3/\text{s}$	47
Figure 4.7 Shell side concentration profile of 39.33 mol/m^3 CO ₂ in Module I for constant inlet gas flow rate of $2.66 \times 10^{-4} \text{ m}^3/\text{s}$ and liquid flow rate of $1.74 \times 10^{-4} \text{ m}^3/\text{s}$	48
Figure 4.8 Concentration profile of 39.33 mol/m^3 CO ₂ in Module II for constant inlet gas flow rate of $2.66 \times 10^{-4} \text{ m}^3/\text{s}$ and liquid flow rate of $1.74 \times 10^{-4} \text{ m}^3/\text{s}$	50
Figure 4.9 Fiber side concentration profile of 39.33 mol/m^3 in ordinary membrane contactor for constant inlet gas flow rate of $2.66 \times 10^{-4} \text{ m}^3/\text{s}$ and liquid flow rate of $1.74 \times 10^{-4} \text{ m}^3/\text{s}$	52
Figure 4.10 Shell side concentration profile of 39.33 mol/m^3 CO ₂ in ordinary membrane contactor for constant inlet gas flow rate of $2.66 \times 10^{-4} \text{ m}^3/\text{s}$ and liquid flow rate of $1.74 \times 10^{-4} \text{ m}^3/\text{s}$	53
Figure 5.1 The effect of module length on acid gas removal.....	61
Figure 5.2 The effect of solvent flow rate on acid gas removal.....	62
Figure 5.4 The effect of pressure on permeate side on acid gas removal.....	64
Figure 5.5 The effect of Henry's constant on acid gas removal.....	66
Figure 5.6 The effect of diffusivity coefficient on acid gas removal	67
Figure 5.7 The effect of number of baffles on acid gas removal	68
Figure 5.8 The effect of permeability of nonporous membrane on acid gas removal.....	69

List of Tables

Table 2.1 Factors influencing permeability of solutes in nonporous polymers	11
Table 2.2 The permeability of carbon dioxide and methane in various polymers	12
Table 4.1 Parameters used in model verifications.....	39
Table 4.2 Parameters in the numerical model.....	44
Table 4.3 CO ₂ inlet and outlet concentration in Module I.....	49
Table 4.4 CO ₂ inlet and outlet concentration in Module II.....	51
Table 4.5 CO ₂ inlet and outlet concentration in ordinary membrane HFMC	54
Table 4.6 CO ₂ concentration changes of mix gas in Module I, II and ordinary HFMC...	55
Table 4.7 CO ₂ concentration change in shell side of Module I, II and ordinary HFMC..	56
Table 4.8 CO ₂ concentration change in Nonporous fibres of Module I and Module II	57
Table 4.9 CO ₂ concentration at gas outlet in Module II with different velocity profiles .	59

Nomenclature

A	Cross area of liquid flow, m^2
C	Mole concentration, mol/m^3
\bar{C}	Average mole concentration, $kgmol/m^3$
D	Diffusion coefficient, m^2/s
D_k	Knudsen diffusion coefficient
H	Henry's constant
h	Height of channel, m
J	Mole flux, mol/s
K	Overall mass transfer coefficient, m/s
k_g, k_m, k_l	Mass transfer coefficient in gas, membrane and liquid, respectively, m/s
L	Length of membrane, m
M_w	Molecular weight
N_g	Mole flow rate of gas, mol/s
P	Pressure, Pa
Per	Permeability coefficient, Barrer
Q	Volumetric flow rate, m^3/s
R	Gas constant, $m^3Pa/kgmolK$
r	Pore radius, m

<i>S</i>	Area of membrane, m ²
<i>Sol</i>	Solubility coefficient in membrane, m ³ (STP)/m ³ Pa
<i>T</i>	Temperature, K
<i>Re</i>	Renolds Number
<i>Gz</i>	Graetz Number
<i>Sh</i>	Sherwood Number
<i>Sc</i>	Schmidt Number
<i>v</i>	Velocity, m/s
<i>w</i>	Width of membrane, m
<i>x</i>	Length coordinate position, m
<i>y</i>	Height coordinate position, m
<i>z</i>	Gas mole percentage, %

Greek symbols

δ	Thickness of membrane, m
μ	Viscosity, Ns/m ²
ρ	Density, kg/m ³
τ	Pore tortuosity
ν	Kinematic viscosity (m ² /s).

Subscripts

G	Gas phase
L	Liquid phase
G_{in}	Gas inlet
L_{in}	Liquid inlet

Chapter 1

Introduction

1.1 Background

Natural gas contains many impurities such as carbon dioxide (CO₂), hydrogen sulphide (H₂S) and water. These contaminants can cause pipe corrosion, hydrate formation, solid formation in Liquefied Natural Gas processes, and other transport problems. Removal of contaminants from natural gas streams before delivery is critical. During the past 30 years, absorption by gas-liquid contactors has dominated natural gas treatment (including CO₂, H₂S removal, dehydration, etc.). Membrane gas absorption devices including membrane contactors can be applied to natural gas processing [1]. Compared to traditional absorption technologies using random or structured packed column to capture contaminants in natural gas, Hollow fiber membrane contactors (HFMC) provides larger available gas-liquid contactor area, a larger overall mass transfer coefficients, and higher removal efficiencies [2]. HFMC are especially useful for offshore platform applications and the small scale gas treatment from remote locations where the small footprint of HFMC is advantageous. This thesis will focus on the fundamentals of HFMC and its application in natural gas treatment.

Membrane technologies first broke into the natural gas processing industry in the

1980s, offering systems for CO₂ removal in competition with the amine absorption. A significant amount of published research work on membrane contactors is related to CO₂ removal. The performance of the membrane contactors was investigated and it was concluded that membrane contactors offer advantages over columns and other conventional mass transfer equipment. These advantages include the followings [3]:

- Significant interfacial area under both high and low flow rates.
- Mass transfer can occur through a membrane without direct contact, which could effectively reduce flooding, foaming and loading.
- Fluids of identical density can be contacted and membranes can be operated in any orientation. No density difference is required between fluids.
- Interfacial area is known and is constant, which allows performance to be predicted more easily when compared with conventional dispersed phase contactors.
- Modular design allows membrane contactors to operate over a wide range of capacities and is easy to install.

1.2 Scope of study

This research aims to demonstrate the performance of HFMC in physical absorption for natural gas processing and techniques to improve the absorption efficiency. CO₂ is one of the most common contaminants in natural gas, so this thesis will focus on the study of novel membrane contactors in CO₂ removal. This research proposes two dual

hollow fiber configurations for the removal of gaseous contaminants using mass balance principles governing the absorption and stripping processes. These two configurations combine absorption and regeneration of solvent into one unit. A certain type of porous membrane is selected according to its permeation ability of the contaminants. The absorbed gaseous contaminant can be stripped into nonporous fibers when a low pressure or vacuum provided inside the nonporous fibers as a driving force. Module I outlined in Figure 1.1 (a) introduces nonporous membranes in the contactor with a low pressure on the permeate side of the membrane. The differential pressure between the inside and outside of the membrane can strip contaminants from the solvent thereby partly regenerate the solvent stream simultaneously with the absorption process. Better absorption efficiencies can be obtained by continuous removal of the gas contaminant components from the solvent. Module II outlined in Figure 1.2 proposes a baffled cross flow HFMC. Wang and Cussler [4] studied the effect of baffles in membrane modules made with hollow fiber fabrics and found that baffles can supply flow perpendicular to fibers. The baffles can also improve mass transfer efficiency by minimizing shell-side bypass and providing a velocity component normal to the membrane surface.

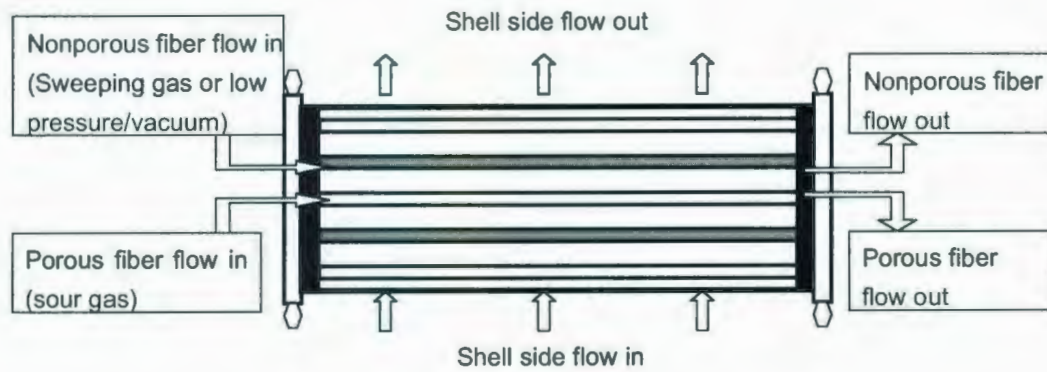


Figure 1.1 Proposed dual membrane contactor: Module I

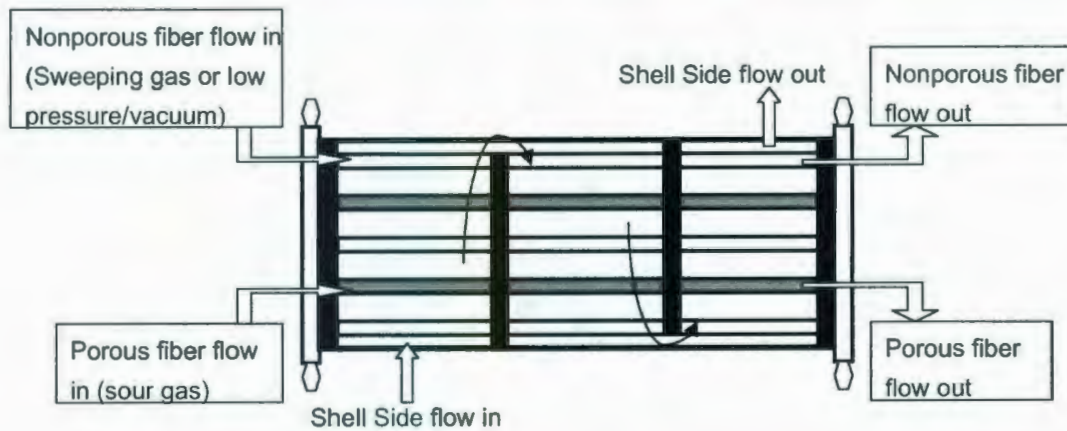


Figure 1.2 Proposed dual membrane contactor with baffles: Module II

1.3 Objectives of study

This research aims to model the performance of two dual hollow fiber configurations for the removal of gaseous contaminants using mass balance principles governing the absorption and stripping processes and compared to single membrane HFMC. Two cross-flow hollow fiber configurations are proposed and the gas contaminant removal efficiencies compared to ordinary single hollow fiber contactors were investigated.

To model the performance of these two cross flow dual HFMC modules, a numerical model based on mass balances are developed to describe the mass transfer in the membrane, liquid phase, as well as gas phase.

Due to the fact that this research only aims at proving the concepts, the model was not verified experimentally at this point. However, to verify the proposed numerical model, the framework of the model was compared to experimental data from a single HFMC (Dindore *et al.*, 2005).

Operating parameters were changed independently to analyze the effects of various parameters on the separation performance, leading to a methodology to determine optimal operational parameters.

1.4 Thesis outline

This thesis is divided into five chapters. Chapter 1 presents a preliminary introduction to the thesis, and gives the concept of HFMC and what is new about this research. In Chapter 2, the fundamentals concerning membrane technology, transport mechanism through membranes and the membrane contactor are presented to give readers a basic understanding of membrane contactor. In Chapter 3, partial differential equations and corresponding initial and boundary conditions are developed to simulate the proposed dual-membrane contactors (including Module I and Module II) and the ordinary single membrane contactor based on single-component absorption. In Chapter 4, the models

are numerically solved using the Crank-Nicholson method. Comparisons between the novel dual-membrane contactors and the single-membrane contactor are carried out. Then Module II is recommended based on industrial consideration. In addition, the fluid dynamics is studied and shows how baffles impact on the mass transfer. In Chapter 5, according to the modeling results, analysis is implemented to check the effect on the performance of various operating parameters. In Chapter 6, summary and conclusions of this thesis as well as some suggestions for future work are presented.

Chapter 2

Introduction to Hollow Fibre Membrane Contactors

This chapter presents a brief introduction to the membrane technology, including membrane separation and membrane absorption and mechanisms of gas molecule diffusing through porous and nonporous membranes. Membranes with different modules and performances are also discussed. Then fundamentals of hollow fiber membrane contactors are explained and the processing of natural gas for CO₂ removal with membranes is described. Previous work on carbon dioxide removal using membrane gas absorption is also reviewed.

2.1 Introduction to Membrane Gas Absorption Technology

2.1.1 Porous and Nonporous Membranes

Membrane gas absorption is a gas–liquid indirect contacting operation. The essential element in the membrane gas absorption process is the membrane contactors. These devices allow mass transfer between gas and liquid phases instead of dispersion of one phase into the other. Different from membrane gas separation, the membrane contactor does not function as a species selective barrier, but rather a material supplying the interfacial area for gas-liquid mass transfer.

Membranes used for gas absorption can be made from various polymers as well as ceramics and carbon fiber materials [5]. Membranes can be categorized into two main groups depending on the pore size: porous and nonporous membranes. According to

the definition of porous adopted by International Union of Pure and Applied Chemistry (IUPAC), the porous membrane refers to membranes with the pores size over 2nm. Membranes without fixed pores or with the pores size less than 2nm are classified as nonporous membranes [5]. The porous membrane acts as a boundary between gas and liquid while the pore size and pore distribution determines the separation performance more than the membrane material itself. On the other hand, the nonporous membrane allows selective and controlled transfer of one species from one phase to another. The material itself determines the separation performance.

Both porous and nonporous membranes have their own advantages and wide applications in gas separation. H. B. Al-saffar et al. [6] compared the performance of porous and nonporous gas-liquid membrane contactors for CO₂ removal and obtained good efficiencies for both membranes. They found that the selectivity of the porous membrane module is determined by the absorbing capacity of the absorbing liquid and also the partitioning characteristics between the two phases. In contrast, the non-porous membrane allows selective and controlled transfer of species from one bulk phase to another; however, the significant mass transfer resistance could reduce the mass transfer rate.

2.2 Transport in Membranes

Transport through a membrane takes place when a driving force is applied. The

driving force can be pressure difference, concentration difference, temperature difference or electrical potential difference. For the natural gas processing application, it mainly involves a pressure or concentration difference as the driving force. When different types of membrane are used for gas separation, various transport mechanisms can be distinguished depending on the structure and material of the membrane.

2.2.1 Transport in Porous Membranes

When gas molecules diffuse through porous membranes, the process involves two main transport mechanisms depending on the membrane pore size. When the pore is large enough ($r > 10\mu\text{m}$), gas molecules collide with each other which results in Poiseuille flow (viscous flow). In Poiseuille flow, the mean free path of gas molecules is very small compared to the pore diameter and no separation is obtained between various gas components (see Fig.2.1). Knudsen diffusion happens when the pores are smaller or when the pressure of the gas is reduced, especially when the mean free path of gas molecules is of the order of the pore size of the membrane. In Knudsen diffusion, the gas molecules collide more frequently with flow boundaries than with other gas molecules. Figure 2.1 shows the schematic drawings of the Poiseuille and Knudsen flows [5].

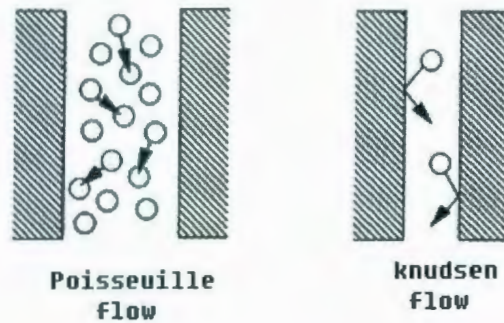


Figure 2.1 Schematic drawings of Poiseuille and Knudsen flows [5]

The mean free path of gas molecules is defined as the average distance traversed by gas molecule collisions; it is proportional to the temperature and inversely proportional to the pressure. Since the mean free path increases as the pressure increases, at low pressure, transport of gases through porous membrane is determined mainly by the Knudsen flow in which the flux can be expressed by the equation:

$$J = \frac{\pi n r^2 D_k \Delta P}{RT \tau \delta} \quad (2.1)$$

where, J is the flux of the gas component; R is gas constant; T is the temperature; r is the pore radius; τ is the pore tortuosity; δ is the thickness of the membrane; n is the number of pores; ΔP is the pressure difference across membrane, D_k is the Knudsen diffusion coefficient, given by:

$$D_k = 0.66r \sqrt{\frac{8RT}{\pi M_w}} \quad (2.2)$$

where, r is the pore radius, and T and M_w are the temperature and molecular weight, respectively. This equation shows that the flux is inversely proportional to the square root of the molecular weight and for a given membrane and pressure difference,

molecular weight of the gas is the only parameter which determines the flux.

2.2.2 Transport in Non-Porous Membranes

For gas absorption, the gas molecules being transported across the membrane dissolve in the nonporous membrane matrix and then diffuse through the nonporous membranes. The concentrations in the membrane are related to the concentrations or partial pressures in the fluid adjacent to the membrane faces. Under steady-state conditions, gas permeation through a nonporous membrane is generally described by the following equation [5]:

$$J_i = \frac{Per_i (P_{o,i} - P_{l,i})}{\delta} \quad (2.3)$$

where, Per_i is the permeability coefficient of component i in the membrane; $P_{o,i}$ and $P_{l,i}$ stand for the partial pressure of component i on the upstream and downstream sides of the membrane respectively; δ is the thickness of the membrane. This equation shows that the flux across a nonporous membrane is proportional to the partial pressure difference and inversely proportional to the membrane thickness. High permeability contributes to a high flux; therefore, membranes with high permeability are preferred in natural gas processing.

This research focuses on the natural gas processing where CO_2/CH_4 is studied as the gas mixture. The permeation abilities of CO_2 and the ideal selectivity of CO_2/CH_4 for some commonly used membranes are compared in Table 2.2. [5]

Table 2.1 The permeability of carbon dioxide and methane in various polymers [5]

Polymer	Per_{CO_2} (Barrer)	Per_{CO_2} / Per_{CH_4}
Polytrimethylsilylpropyne	33100	2.0
Silicone rubber	3200	3.4
Natural rubber	130	4.6
Polystyrene	11	8.5
Polyamide (Nylon)	0.16	11.2
Poly (vinyl chloride)	0.16	15.1
Polycarbonate (Lexan)	10.0	26.7
Polysulfone	4.4	30.0
Polyethyleneterephthalate (Mylar)	0.14	31.6
Cellulose acetate	6.0	31.0
Poly (ether imide) (Ultem)	1.5	45.0

* 1 Barrer = $0.76 \cdot 10^{-17} \text{ m}^3 \text{ (STP) m m}^{-2} \text{ s}^{-1} \text{ Pa}^{-1}$

2.2.3 Membrane Modules

Depending on the types of membranes in contactors, the membrane module can be classified into plate and frame, spiral wound and hollow fiber modules. In the plate in frame module (see Figure 2.2), the membranes are arranged in layers with feed side facing each other. The density is about 100 to 400 m^2/m^3 . During process, feed flows

from its sides and permeate comes out from the top and the bottom of the frame.

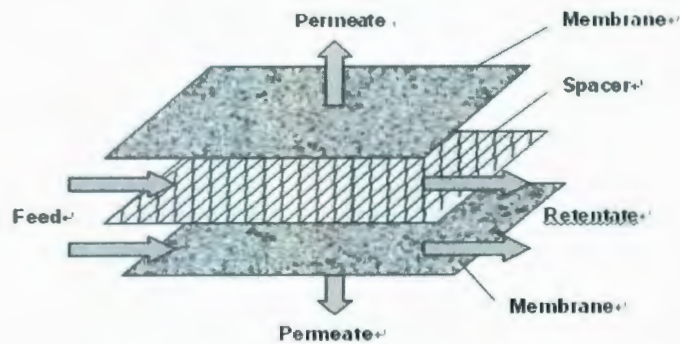


Figure 2.2 Schematic drawing of a plate-and-frame module [5]

Spiral wound module (see Figure 2.3) is formed from a plate and frame sheet wrapped around center collection pipe, the density is about 300 to 1,000 m^2/m^3 . Feed flows axially on the cylindrical module and permeate through the membrane sheet into the central pipe. The Spiral wound module has a wide application in gas processing due to its high pressure durability.

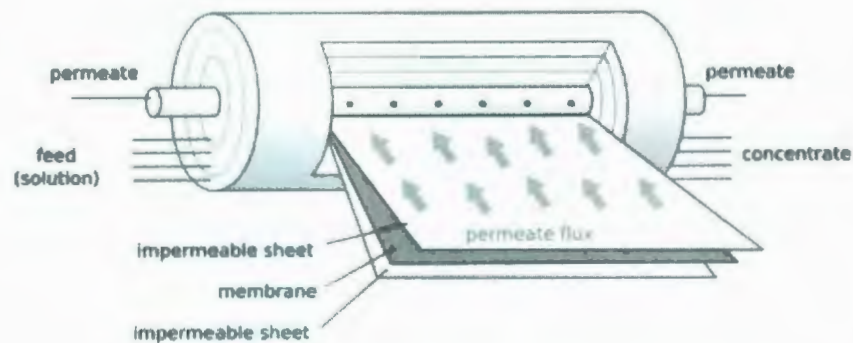


Figure 2.3 Schematic drawing of a spiral-wound module [7]

Hollow fiber membrane contactors have become an attractive technology for gas

separation where space is limited. They allow large areas of membrane to be packaged into compact membrane modules with the density about $600\text{-}1,200\text{ m}^2/\text{m}^3$. The interfacial area for liquid and gas contacting of the hollow fiber module is much higher than spiral wound and plate-form modules. This advantage proved decisive in the choice of membranes for the separation of nitrogen from air, which was an early large-scale membrane gas separation process [2].

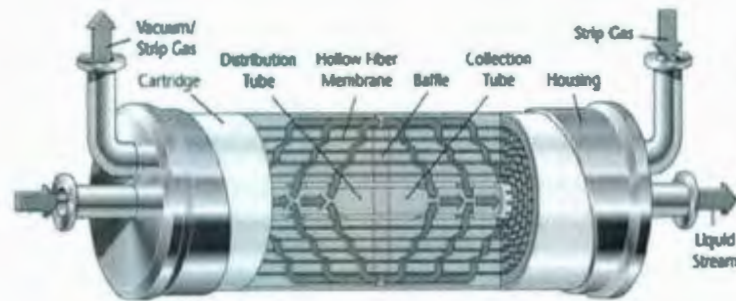


Figure 2.4 Schematic drawing of a HFMC module :Liqui-Cel® contactor [2]

2.2 Hollow Fiber Membrane Contactors (HFMC)

Although a number of membrane module geometries are possible for natural gas separation, hollow fiber modules have received the most attention. HFMC offers large membrane surface per module volume. It is smaller than other type of membranes in volume but has a higher performance [2]. Figure 2.5 compares the surface area to volume ratios of various membrane modules and shows that membrane with hollow fiber fabrics has the highest interfacial area.

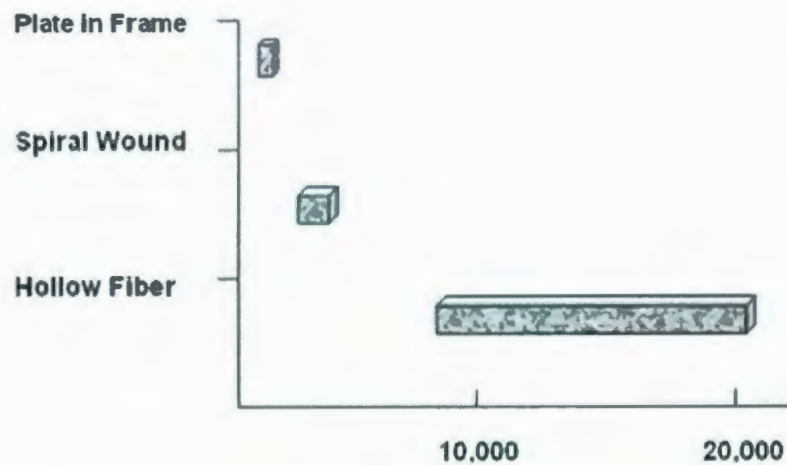


Figure 2.5 Surface areas to volume ratios of various membrane module configurations [1].

2.2.1 Flow Direction in Hollow Fiber Membrane Contactors

Based on the flow directions of the gas and liquid phase, the HFMC can be used in two different modes of operation: parallel flow mode and cross flow mode. The parallel flow refers to the flow of both phases in parallel to the arrangement direction of the fibers with both fluids flowing either in same direction (co-current) or in opposite directions (countercurrent). In cross-flow mode, the shell-side fluid flows perpendicularly to the axis of fiber. Thus the two fluids flow across each side of membrane at right angles. The operation principle of these modes of operation is shown in Figure 2.6 (a) and (b).

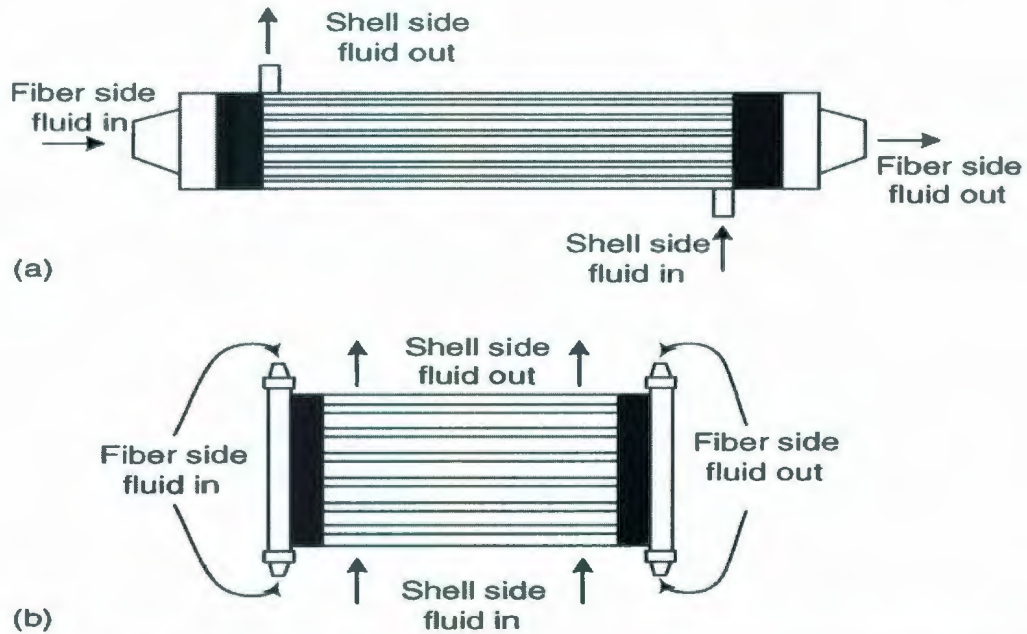


Figure 2.6 (a) Parallel-flow hollow fibre module; (b) cross-flow hollow fibre module [3]

Wang and Cussler explained that the conventional parallel flow mode offers larger transfer area and is preferred when the membrane or the tube side boundary layer resistance controls [4]. However, the cross-flow mode is preferred when shell side mass transfer resistance is significant [19]. The normal flow to the fibers leads to higher mass-transfer coefficients, minimized shell-side channeling and lower shell-side pressure drop compared to parallel flow. Baffled modules are also studied and are found to have a higher efficiency as the number of baffles increases, but pressure drop increases as well. Wang and Cussler [4] looked at the effect of the number of baffles on mass transfer performance in stripping oxygen from water and explained that the highest oxygen removal was achieved using countercurrent flow with five baffles, cross flow with no baffles was superior to concurrent flow with two.

2.2.2 Wetted and Non-wetted Mode

Porous membranes can be hydrophobic or hydrophilic. Two modes of operation are possible in membrane contactors: wetted mode and non-wetted mode. If the liquid phase is aqueous and a hydrophilic membrane is used, wetted mode occurs when the pores are filled with liquid. When a hydrophobic membrane is used with an aqueous solvent, the membrane is under the non-wetted mode, i.e. the pores are filled with gases and the liquid does not wet the membrane. Non-wetted mode is usually preferred to take advantage of the higher diffusivity in the gas; however, wetted mode may be preferred if there is a fast or instantaneous liquid phase reaction and as a result the gas phase resistance controls [6, 8]. Figure 2.7 gives a schematic description of the two modes.

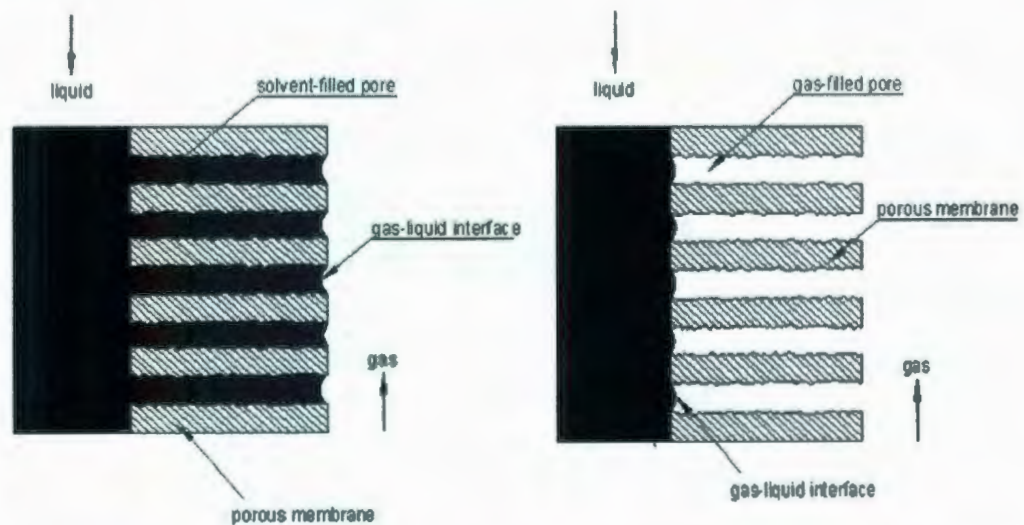


Figure 2.7 Wetted and Non-wetted mode of membrane-based gas-liquid contacting [8]

Karoor and Sirkar studied the absorption of pure CO_2 , pure SO_2 , and CO_2 from CO_2/CH_4 mixtures, and SO_2 from SO_2/air mixtures into water using parallel flow with

module employing microporous polypropylene fibers under both wetted and non-wetted mode. As expected, the authors found that better absorption were obtained under non-wetted mode for both CO₂ and SO₂ [8].

2.2.3 Overall Mass Transfer

In general, the gas absorption process can be categorized as either a physical or a chemical absorption or a combination of the two. In the case of physical absorption, the gaseous solute is physically dissolved in the liquid phase, whereas in the case of chemical absorption the gaseous solute reacts chemically in the liquid phase. This thesis will focus on the physical absorption.

In physical absorption, the transfer of gas molecules from gas phase to the liquid consists of three steps shown in Figure 2.8:

1. Transfer from bulk of the gas phase to membrane,
2. Transfer of a solute through the membrane pores to the liquid interface, and
3. Transfer from membrane into bulk of the liquid phase.

The flux can be expressed in the following expression:

$$J_i = K_i \Delta C_i \quad (2.4)$$

where, J_i is the flux of component i ; ΔC_i is the bulk concentration difference of component i ; K_i , overall mass transfer coefficient, can be related to the individual mass transfer resistance due to gas, membrane, and liquid phases [9].

$$\frac{1}{K_i} = \frac{H_i}{k_{g,i}} + \frac{H_i}{k_{m,i}} + \frac{1}{k_{l,i}} \quad (2.5)$$

where, $k_{g,i}$, $k_{m,i}$, $k_{l,i}$ represent the mass transfer coefficients in gas, membrane and liquid phases, respectively; H_i denotes the dimensionless Henry's constant ($C_{g,i}H_i = C_{l,i}$). The individual mass transfer coefficients $k_{g,i}$ and $k_{m,i}$ are mainly determined by the geometry and the flow conditions in membrane contactor and various correlations have been derived in previous literatures [10,11]. The mass transfer resistance of membrane is mainly determined by diffusion of the solute through the membrane pores, since the membrane and the gas phase resistances can be neglected in non-wetted gas absorption, mass transfer is mainly controlled by liquid phase under this mode.

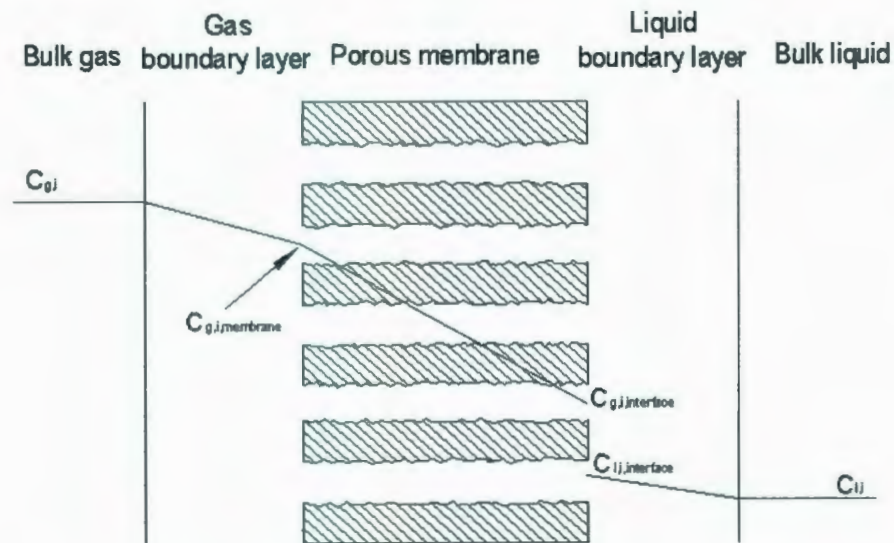


Figure 2.8 Mass transfer regions in a membrane contactor [9]

2.3 Natural Gas Processing with Membranes

Natural gas attracted significant attention in recent years. As other fossil fuels, natural

gas needs to be treated before delivery and transportation. One of the most common contaminants is CO₂, which can be combined with water to form corrosive carbonic acid. Currently, amine system is the dominant technology for CO₂ removal; however, it requires large space commitment and energy to run the boiler and chemical residues are very difficult to deal with. Membrane technology competes most directly against absorption for carbon dioxide removal due to its compactness and simple environmental operations [12]. It requires less than half the foot print area and operating weight and less than fifth of the volume of the conventional absorption system [13].

Membranes were first applied into the natural gas processing industry in the 1980s, offering systems for CO₂ removal in competition with amine absorption[1]. Cussler and his coworkers [14] initially studied the absorption of a variety of gases in alkaline medium using membrane hollow fiber modules for industrial applications. They found that the membrane mass transfer resistance can be neglected and the liquid-side mass transfer resistance controlled the CO₂ absorption in aqueous liquid side. Dindore *et al.* studied the performance of micro-porous cross flow in HFMC and developed a physical absorption model by describing the gas flow with the mixing-cell model; they found various mass transfer effects including the physical solvent on the performance of membrane and application of HFMC in natural gas separation [15,16].

In conventional gas treatment processes, the absorption and regeneration systems are separate due to different operating conditions. However, on offshore applications, merging the contactor and stripper into one unit operation would be preferred as this would decrease the equipment footprint. In response to this, Wang *et al.* proposed a flat sheet configuration where porous and nonporous membranes were incorporated into a single unit within which the circulating solvent is partially regenerated during the absorption, this configuration can potentially reduce the overall size and increase the efficiency of gas processing facilities, which would make them more suitable for offshore applications [17].

Chapter 3

Mathematical Model Development

The main aim of this research was to study the cross flow dual membrane contactors using numerical model. In this chapter, a novel mathematical modeling approach to predict performance of two proposed cross flow hollow fiber dual membrane contactors (Module I and II) and also the ordinary single hollow fiber contactor.

Material balance has been applied to analysis the mass transfer between liquid phase and gas phase through membranes. In general, the total amount of contaminants in natural gas should be equal to those transferring from gas phase into the liquid phase plus those permeate through nonporous membrane into the nonporous hollow fibers.

The mass transfer in each phase can be described through diffusion and permeation equations, respectively.

A mixture of CH_4 and CO_2 is used in the modeling with pure water as the absorbent liquid. Because CH_4 , due to its very small water solubility compared to CO_2 , does not significantly take part in the absorption, the modeling can be reduced to a single-component absorption process. The experiments are conducted with water in the shell side and mixture gas flowing through the fibers since passing the phase with the controlling transfer resistance on the shell side gives a better transfer performance [16].

3.1 Assumptions for Model Development

The models are constructed based on the following simplifying assumptions: [5-7]

1. The membrane contactor is operated under steady state and isothermal conditions.
2. The physical properties including diffusion coefficient, Henry's constant, density, viscosity etc. are constant along the membrane.
3. Henry's law is applicable at the interface of gas and liquid, and equilibrium is instantaneously obtained.
4. No chemical reaction is involved, only physical mass transfer is modeled.
5. The liquid flow between two baffles is fully developed laminar flow.
6. The x -direction diffusion and y -direction convection are negligible.
7. The membranes are under the non-wetted mode (gas-filled pores).
8. The pressure in gas phase is constant along the membrane.

In this thesis, pure CH_4 is used as sweeping gas. In Module I and II, the solvent will inevitably evaporate through desorption membrane due to the low pressure employed on permeate side, so a nonporous membrane with a low permeability to the solvent should be chosen to make the vaporization negligible compared to the flux of CO_2 . CO_2 is denoted by the contaminant in the following formula.

3.2 Mass Transfer Fundamentals

To model the performance of the cross flow dual hollow fiber membrane contactors in

Module I and II, a numerical model of cross-flow module based on mass balance involving a set of partial differential equations are developed to describe the mass transfer in the membrane, liquid phase as well as gas phase.

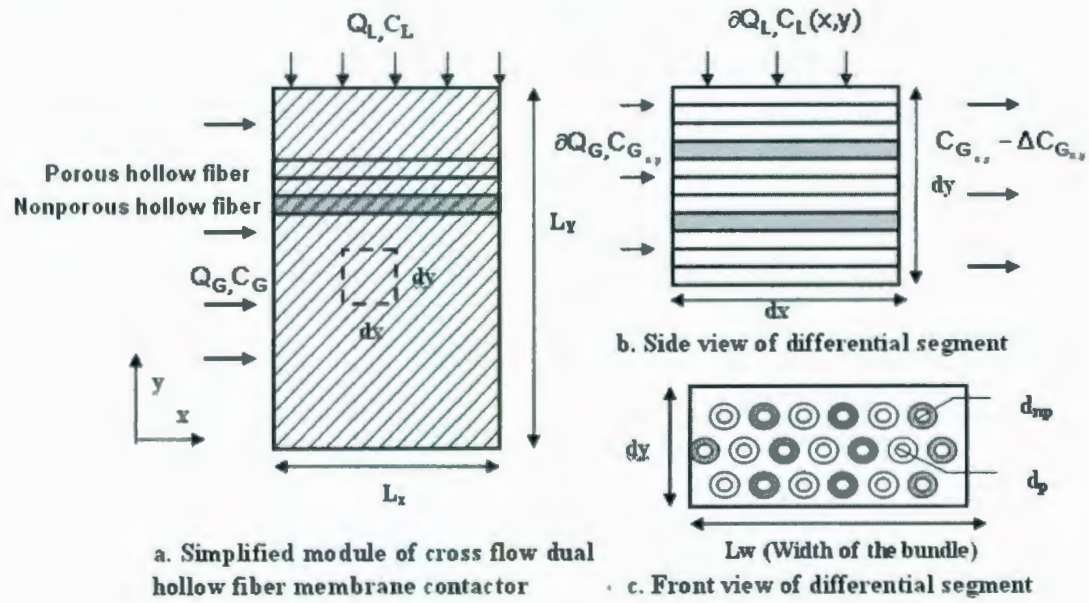


Figure 3.1 Cross section and modeling parameters in cross flow membrane contactor

3.2.1 Overall Mass transfer in the liquid phase

Applying material balance on a differential segment of the module in Figure 3.1, based on above assumptions, the change of mass in liquid phase is due to loss of mass in gas in porous hollow fiber and gain of mass in the nonporous hollow fiber, the overall mass balance therefore can be expressed as follows:

$$\partial Q_L \Delta C_L = \partial Q_G \Delta C_G - \partial q_{np} \quad (3.1)$$

Taking a differential segment of the module, according to material balance, the number of moles of contaminant absorbed by the solvent is equal to that of diffusing through the boundary. The mass balance in liquid phase hence can be derived as:

$$\frac{dx}{L_x} Q_L \partial C_L = k_L dA_p (HC_G - C_L) - k_L dA_{nP} (C_L - C_{out}) \quad (3.2)$$

where, dA_p denotes transfer area between gas and liquid in porous membrane given in the following Equation 3.3, C_{out} refers to the concentration in sweep gas or the vacuum.

$$dA_p = A_p N_p = \pi d_p L_p \times \frac{(1 - \alpha_p) L_W dx dy}{\frac{\pi d_p^2}{4} dx} \quad (3.3)$$

where, $(1 - \alpha_p)$ denotes the packing fraction of the module.

Combing Equations (3.2) and (3.3), the following partial differential equation can be obtained:

$$\frac{\partial C_L}{\partial y} = M_p (HC_G - C_L) - M_{nP} (C_L - C_{out}) \quad (3.4)$$

$$\text{where, } M_p = \frac{4(1 - \alpha_p) L_W L_x K_L}{d_p Q_L}; \quad M_{nP} = \frac{4(1 - \alpha_{nP}) L_W L_x K_L}{d_{nP} Q_L}$$

3.2.2 Gas phase mass balance within porous membranes

The transfer of contaminant molecules from gas phase to the liquid consists of three steps: transfer from bulk of the gas phase to the membrane; diffusion through the gas-filled pores and transfer from membranes into bulk of the liquid phase. The mass balance in the gas phase can be expressed as:

$$\partial Q \Delta C_G = kdA_p (HC_G - C_L) \quad (3.6)$$

where, k is the overall mass transfer coefficient equal to k_L in this model since the membrane and the gas phase resistance can be neglected in non-wetted gas absorption, mass transfer is controlled by liquid phase under this mode. k_L can be obtained from Sherwood number (kd/D) and empirical equations [18]:

$$Sh = 0.18 Re^{0.86} Sc^{0.33} \quad (3.7)$$

where, the Reynolds number is calculated from the outer fiber diameter, the kinematics viscosity and a superficial velocity; Schmidt number (ν/D) dependence is verified by other experiments [19]. Combining Equation 3.3, we have:

$$\frac{\partial C_G}{\partial x} = M_G (C_L - HC_G) \quad (3.8)$$

$$\text{where, } M_G = \frac{4(1 - \alpha_p)L_x L_w k_L}{d_p Q_G}$$

3.2.3 Gas phase mass balance within nonporous membranes

The gaseous contaminant absorbed in the liquid phase permeates through the nonporous membrane by diffusion mechanism. The flux is proportional to partial pressure difference and inversely proportional to the membrane thickness. The mass transfer through nonporous membrane can be described as follows according to the basic diffusion mass transfer:

$$\partial q_{np} = kdA_{np} (C_L - C_{snp}) \quad (3.10)$$

where, dA_{np} denotes transfer area between gas and liquid in porous membrane given in the following equation, C_{snp} is the contaminant concentration at the surface of

nonporous membrane.

Diffusion through nonporous membrane of thickness t_{np} can also be described as:

$$\partial q_{np} = \frac{K_{Per}}{t_{np}} \left(\frac{C_{snp} RT}{H} - P_{out} \right) \pi d_{np} \Delta x \quad (3.11)$$

where, k_{per} denotes nonporous permeability for gas contaminants and the membrane, P_{out} refers to the pressure in the nonporous membrane. Thickness t_{np} is assumed to be small and therefore the outer and inner surface areas are equal.

Combining Equations 3.10 and 3.11, the expression for C_{snp} can be obtained as follows:

$$C_{snp} = \frac{C_L + \frac{k_{per}}{k_L t_{np}} P_{out}}{1 + \frac{k_{per}}{k_L t_{np}} \frac{RT}{H}} \quad (3.12)$$

where H denotes the Henry constant and T is the temperature under which the experiment are conducted.

Similar to the Module I and II, the same model can also be applied to the baffled module, but mass transfer for each segment between the baffles in Module II can be modeled by above partial differential equations (Equations 3.4 and 3.8); the outlet concentrations of the previous segment in both gas and liquid phases will be parts of the initial and boundary conditions for the next segment. Starting from the gas inlet, concentrations through all of the segments can be calculated in the module. Additionally, in gas phase, the concentration distribution of contaminant in the y

direction can be negligible compared to liquid phase since the diffusion coefficient in gas phase is typically much larger than in liquid phase. That is, gas phase is completely mixed in y direction and the concentration profile of contaminant in gas phase is a function of only x .

3.3 Module Development

3.3.1 Module I

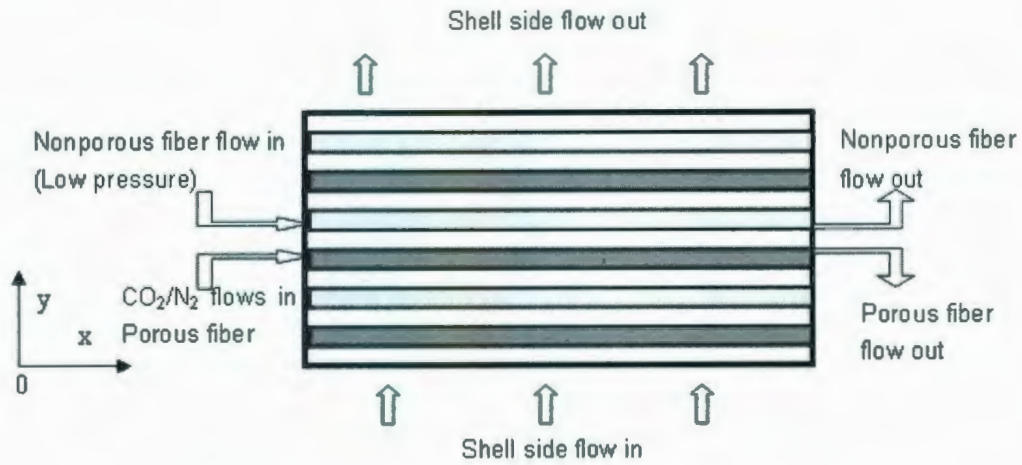


Figure 3.2 Schematic structure of dual HFMC: Module I

The number of moles of contaminant absorbed by the solvent is equal to that of diffusing through the boundary; the mass balance in liquid phase hence can be derived as Equation 3.2.

$$\frac{dx}{L_x} Q_L \partial C_L = k_L dA_P (HC_G - C_L) - k_L dA_{nP} (C_L - C_{out})$$

The partial differential equation Equation 3.4 is also derived as shown in Section 3.1.1:

$$\frac{\partial C_L}{\partial y} = M_p (HC_G - C_L) - M_{nP} (C_L - C_{out})$$

The contaminant concentration in sweeping gas C_{out} is approximately equal to the concentration on the surface of nonporous membrane C_{snp} , so equation 3.4 can also be expressed as:

$$\frac{\partial C_L}{\partial y} = M_p (HC_G - C_L) - M_{nP} (C_L - C_{snp}) \quad (3.16)$$

Combining Equations 3.12 and 3.16, the following equation can be obtained:

$$\frac{\partial C_L}{\partial y} = M_p (HC_G - C_L) - M_{nP} \left(C_L - \frac{C_L + \gamma_o}{\gamma_h} \right) \quad (3.17)$$

$$\text{where, } \gamma_o = \frac{k_{per}}{k_L t_{np}} P_{out}, \quad \gamma_h = \frac{k_{per}}{k_L t_{np}} \frac{RT}{H}$$

At gas entrance where x is equal to zero, C_L is a function of y only, thereby, the boundary condition to Equation 3.17 can be expressed as:

$$x=0; \quad \frac{\partial C_L}{\partial y} \Big|_{x=0} = M_p (HC_{GIN} - C_L \Big|_{x=0}) - M_{nP} \left(C_L \Big|_{x=0} - \frac{C_L + \gamma_o}{\gamma_h} \right) \quad (3.18)$$

Inlet condition:

$$y=0; \quad C_{G_i} = C_{G_{in,i}} \quad (3.19)$$

and

$$\frac{\partial C_G}{\partial x} = M_G (C_L - HC_G) \quad (3.8)$$

Hence, the boundary condition to Equation 3.8 can be defined as:

$$y=0; \quad \frac{\partial C_G}{\partial x} \Big|_{y=0} = M_G (C_L - HC_G \Big|_{y=0}) \quad (3.20)$$

Inlet condition:

$$y=0; \quad C_{L_i} = C_{L_{in,i}} \quad (3.21)$$

The following second order partial differential equations can be obtained by combining the mass transfer equations in both gas side and liquid side (Equations 3.8 and 3.17):

$$\frac{\partial^2 C_G(x, y)}{\partial x \partial y} + \left(\frac{M_{np} r_h}{1 + r_h} + M_p \right) \frac{\partial C_G(x, y)}{\partial x} + M_G H \frac{\partial C_G(x, y)}{\partial y} + \frac{H}{1 + r_h} (M_G M_{np} r_h C_G(x, y) - M_G M_{np} r_o) = 0$$

(3.22)

Boundary conditions are as follows:

$$x = 0, C_{Gi} = C_{Gin}$$

$$y = 0, C_{Gi} = \frac{C_{Lin}}{H_i} (C_{Gin, j} \Big|_{y=0} - \frac{C_{Lin}}{H_i}) e^{-M_G H_i x} \quad (3.23)$$

Equation 3.23 is the analytical solution to Equation 3.20.

Initial conditions:

$$y = 0, C_{Lin} = 0 \quad (3.24)$$

Since the solvent in the shell side is pure water in this proposed model, the contaminant concentration is equation to zero at the shell side inlet.

Then C_L is numerically calculated from Equation 3.8, which can change into the form below:

$$C_L(x, y) = H_i C_G(x, y) - \frac{1}{M_G} \frac{\partial C_G(x, y)}{\partial x} \quad (3.25)$$

3.3.2 Module II

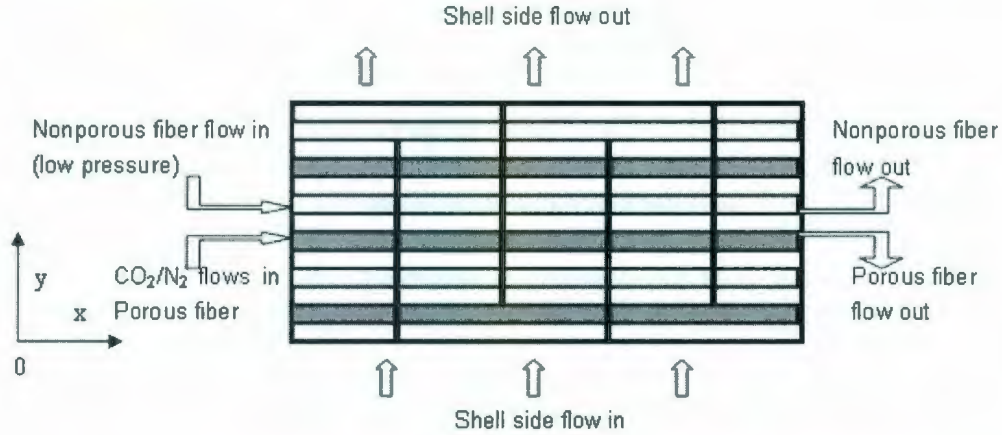


Figure 3.3 Schematic structure of dual HFMC: Module II

Similar to Module I, the overall mass transfer in Module II can also be described by combining mass transfer equations in gas and liquid phases:

$$\frac{\partial^2 C_G(x, y)}{\partial x \partial y} + \left(\frac{M_{np} r_h}{1 + r_h} + M_p \right) \frac{\partial C_G(x, y)}{\partial x} + M_G H \frac{\partial C_G(x, y)}{\partial y} + \frac{H}{1 + r_h} (M_G M_{np} r_h C_G(x, y) - M_G M_{np} r_o) = 0$$

Boundary conditions:

$$x = 0, C_{Gi} = C_{Gin}(y) \quad (3.26)$$

$$y = 0, C_{Gi} = \frac{\bar{C}_{Lin}}{H_i} (C_{Gin,j} \Big|_{y=0} - \frac{\bar{C}_{Lin}}{H_i}) e^{-M_G H_i x} \quad (3.27)$$

Different from Configuration 1, Equation 3.26 will be a function of y in the baffled module; it is a constant only at the entrance of the first module. Each section between the baffles in Module II is assumed as an individual module, and the C_{Lin} therefore is assumed to be the average C_L in Equation 3.27 which is calculated at each module.

Initial conditions:

$$y = 0, C_{Lin} = C_{Lin,j} \quad (3.24)$$

C_{Lin} equals to 0 only at the entrance of the first baffle.

Then the concentration change in liquid phase can also be numerically calculated from the following equation, which can be calculated as the initial condition for the next module:

$$C_L(x, y) = H_i C_G(x, y) - \frac{1}{M_G} \frac{\partial C_G(x, y)}{\partial x}$$

3.3.3 Ordinary Hollow Fiber Contactor

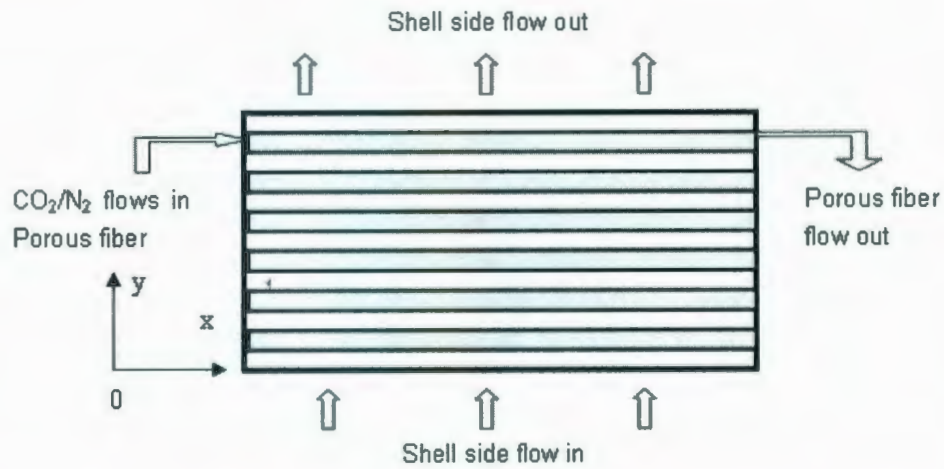


Figure 3.4 Schematic structure of Ordinary single membrane HFMC

The same analysis is applied to the ordinary hollow fiber contactor which only contains porous membrane in the module, the describing partial differential equation then changes to:

$$\frac{\partial^2 C_G(x, y)}{\partial x \partial y} + M_p \frac{\partial C_G(x, y)}{\partial x} + M_G H \frac{\partial C_G(x, y)}{\partial y} = 0 \quad (3.28)$$

Boundary conditions:

$$x = 0, C_{Gi} = C_{Gin}$$

$$y=0, C_{Gi} = \frac{C_{Lin}}{H_i} (C_{Gin,j} \Big|_{y=0} - \frac{C_{Lin}}{H_i}) e^{-M_c H_i x} \quad (3.23)$$

Initial conditions:

$$y=0, C_{Lin} = 0 \quad (3.24)$$

3.4 Computational Fluid Dynamics (CFD)

In the mass transfer between gas and liquid phases, the liquid velocity plays an important part in influencing the mass transfer coefficient since the controlling transfer resistance mainly relies on the liquid side. According to literature, fully developed laminar flow in liquid phase is a reasonable assumption for the study of membrane contactors [20-22], however, the proposed modules in this study have relatively small dimensions in all x, y and z directions, and the liquid velocity is assumed to be constant as the fluids pass through the modules. To investigate the influence of velocity change in shell side to the mass transfer phenomena, especially in the baffled module, hydrodynamics for the liquid adjacent to the membrane in Module II have been studied using a CFD simulation package. The CFD simulation provides visualization of fluid flow patterns for the baffled module. In this work, FLUENT v.6 was used to predict the velocity profile of the fluid in the shell side in Module II. The velocity data from FLUENT v.6 were fit to representative equations and used in the MAPLE code to qualitatively observe the influence of fluid flow on mass transfer coefficients. The velocity of gas phase in the fibers is assumed to be constant due to its low viscosity and small fiber diameters.

The presence of fibers in Module II makes it impossible to simulate the velocity field in 2-D mode. To simplify the further calculation, the fibers were not taken into consideration during grid generation in this work. The velocity changes of liquid in shell side were simulated in empty shell by FLUEN v.6. This assumption may result in deviation between model and real data, but the impact of baffles on velocity can still be clearly demonstrated.

Chapter 4

Solutions to Model Equations

This chapter compares the performance of the proposed dual hollow fiber membrane modules and demonstrates the improvement in performance compared to the ordinary HFMC. The partial differential equations are solved numerically with the Crank-Nicholson method using MAPLE. The predicted absorption efficiency from the model was compared to experimental data [16] to verify the numerical model. The CO₂ removal efficiency from CO₂- CH₄ mixture gases of the novel dual-membrane Module I and Module II are compared to the ordinary single-membrane contactor under the same operating conditions. In addition to nonporous membrane, baffles are also introduced into Module II to determine if the mass transfer can be increased by minimizing shell-side bypass and increasing liquid velocity. To further investigate how the baffles impact the mass transfer, the CO₂ removal efficiency of the baffled module under constant solvent flow rate was compared to that under varying solvent flow rate at the last part of this chapter.

4.1 Numerical Solution

It is known that not all partial differential equations can be solved analytically and that numerical solution can be a very good approximation if implemented correctly. The complexity of the partial differential equation and boundary conditions makes the

numerical method a preferred solution technique for this problem compared to analytical methods. MAPLE[®] provides 11 standard numerical methods to PDEs. The specified method can be customized according to numerical boundary conditions and startup schemes. It is known that both explicit and implicit methods can be used in the solving of the partial differential equations though implicit method provides more accuracy. The Crank-Nicholson method is used in Maple in this work due to its unconditional stability for many problems. The Crank-Nicholson method requires PDEs that are odd order in space and numerical boundary conditions need to be specified so that each boundary has the same total number of conditions. For second order PDE, no numerical boundary conditions were required, but the same number of conditions on each boundary must be specified [26]. From the numerical solution, the concentration distribution of the CO₂ in each phase can be obtained.

For the Model I, Equation 3.22 together with boundary conditions and initial conditions (as described in chapter 3) can be solved by Crank-Nicholson method in Maple:

$$\left\{ \begin{array}{l} \frac{\partial^2 C_G(x,y)}{\partial x \partial y} + \left(\frac{M_{np} r_h}{1+r_h} + M_p \right) \frac{\partial C_G(x,y)}{\partial x} + M_G H \frac{\partial C_G(x,y)}{\partial y} + \frac{H}{1+r_h} (M_G M_{np} r_h C_G(x,y) - M_G M_{np} r_o) = 0 \\ x=0, C_{Gi} = C_{Gin} \\ y=0, C_{Gi} = \frac{C_{Lin}}{H_i} (C_{Gin,j} \Big|_{y=0} - \frac{C_{Lin}}{H_i}) e^{-M_G H_i x} \\ y=0, C_{Lin} = 0 \\ \frac{\partial C_L}{\partial y} = M_p (H C_G - C_L) - M_{nP} (C_L - C_{snp}) \end{array} \right.$$

Similarly, the following equation groups, which describe the performance of Module

II can be solved in the same way:

$$\left\{ \begin{array}{l} \frac{\partial^2 C_G(x, y)}{\partial x \partial y} + \left(\frac{M_{np} r_h}{1 + r_h} + M_p \right) \frac{\partial C_G(x, y)}{\partial x} + M_G H \frac{\partial C_G(x, y)}{\partial y} + \frac{H}{1 + r_h} (M_G M_{np} r_h C_G(x, y) - M_G M_{np} r_o) = 0 \\ x = 0, C_{Gi} = C_{Gin}(y) \\ y = 0, C_{Gi} = \frac{\bar{C}_{Lin}}{H_i} (C_{Gin, j} \Big|_{y=0} - \frac{\bar{C}_{Lin}}{H_i}) e^{-M_G H_i x} \\ \frac{\partial C_L}{\partial y} = M_p (H C_G - C_L) - M_{nP} (C_L - C_{snp}) \end{array} \right.$$

The following equation groups are solved to describe the mass transfer in ordinary membrane contactor, which only contains porous membrane in the module.

$$\left\{ \begin{array}{l} \frac{\partial^2 C_G(x, y)}{\partial x \partial y} + M_p \frac{\partial C_G(x, y)}{\partial x} + M_G H \frac{\partial C_G(x, y)}{\partial y} = 0 \\ x = 0, C_{Gi} = C_{Gin} \\ y = 0, C_{Gi} = \frac{C_{Lin}}{H_i} (C_{Gin, j} \Big|_{y=0} - \frac{C_{Lin}}{H_i}) e^{-M_G H_i x} \\ y = 0, C_{Lin} = 0 \end{array} \right.$$

4.2 Model Validation

To verify the numerical solution, the numerical model was applied to the module developed by Dindore *et.al* (2005) (Shown in Figure 4.1) in which absorption solvent goes through the fibers and the mixture gas goes through the shell side (i.e. only one type of membrane is used). The predicted absorption efficiencies from model were compared to experimental data [16].

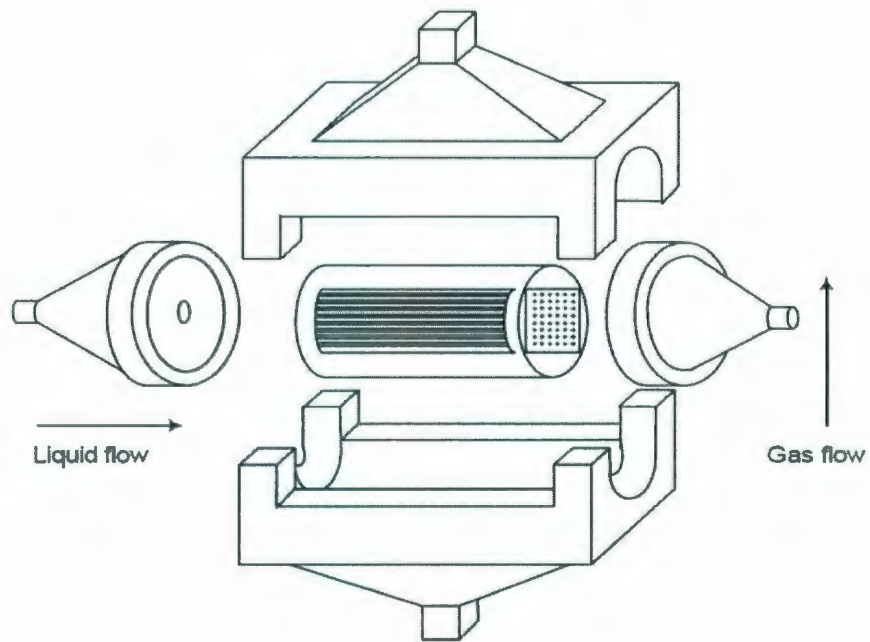


Figure 4.1 Cross flow membrane Module developed by Dindore *et al.* [16]

The PDEs are numerically solved in MAPLE combining the boundary conditions and initial conditions, the values of parameters used in the calculations are listed in Table 4.1, which are consistent with those in experiments.

Table 4.1 Parameters used in model verifications [16]

Parameter	Value
Channel height (m)	0.1
Dimension of module (m ²)	0.1×0.1
Solvent (H ₂ O) flow rate (10 ⁻⁴ m ³ /s)	1.74
CO ₂ inlet concentration (mol/m ³)	14.62
Henry's constant (CO ₂ in H ₂ O)	0.78
Diffusivity of CO ₂ in H ₂ O (10 ⁻⁹ m ² /s)	1.8
Temperature (K)	293.0
Pressure of mixture gas (10 ⁵ PaA)	1
Number of Porous Fiber	4900
Voidage	0.615
Fiber Type	Polypropylene

4.2.1 Mass Transfer Coefficient on Fiber Side

In CO₂ removal from CO₂-N₂ mixture using water, earlier measurements [23] showed little mass transfer resistance across the membrane or in the gas phase, so the individual mass transfer coefficient in the water is used in place of the overall mass transfer coefficient. Several correlations have been developed to predict the mass transfer coefficient in a cross flow hollow fiber membrane contactor with solvent

flowing through the fiber for both fiber and shell side flow [24]. Two asymptotic correlations based on the heat transfer analogy of the Graetz-Leveque equations are widely used to predict the mass transfer coefficient on the fiber side [17-18].

$$Sh = \sqrt[3]{1.67Gz} \quad Gz > 20 \quad (4.1)$$

$$Sh = \sqrt[3]{3.67^3 + 1.63^3} Gz \quad 10 < Gz < 20 \quad (4.2)$$

$$Sh = 3.67 \quad Gz < 10 \quad (4.3)$$

Equation 4.1 is the well-known Leveque solution, which is widely used for predicting fiber side mass transfer coefficient of gas and liquid hollow fiber fabric contactors, where the Sherwood number is a function of the mass transfer coefficient, the fiber outside diameter and a diffusion coefficient of CO₂ in water whereas the Graetz number can be calculated from mass diffusivity (*D*), fiber diameter (*L*), Reynolds number (*Re*) and Schmidt number (*Sc*) [27].

$$G_z = \frac{D}{L} Re.Sc$$

The Schmidt number is defined as the ratio of viscosity (*v*) and mass diffusivity (*D*) [29].

The Leveque solutions of mass transfer coefficient are compared to experiments measurements [16] in Figure 4.2 for Polypropylene membrane with water as the absorption solvent. It is clear from the figure that the Leveque solution agrees well with the experimental data and used to predict the fiber side transfer coefficient in case of water. Moreover, it also shows the effect of liquid flow rate on mass transfer coefficient and verifies the controlling resistance to mass transfer process is indeed in

the liquid phase.

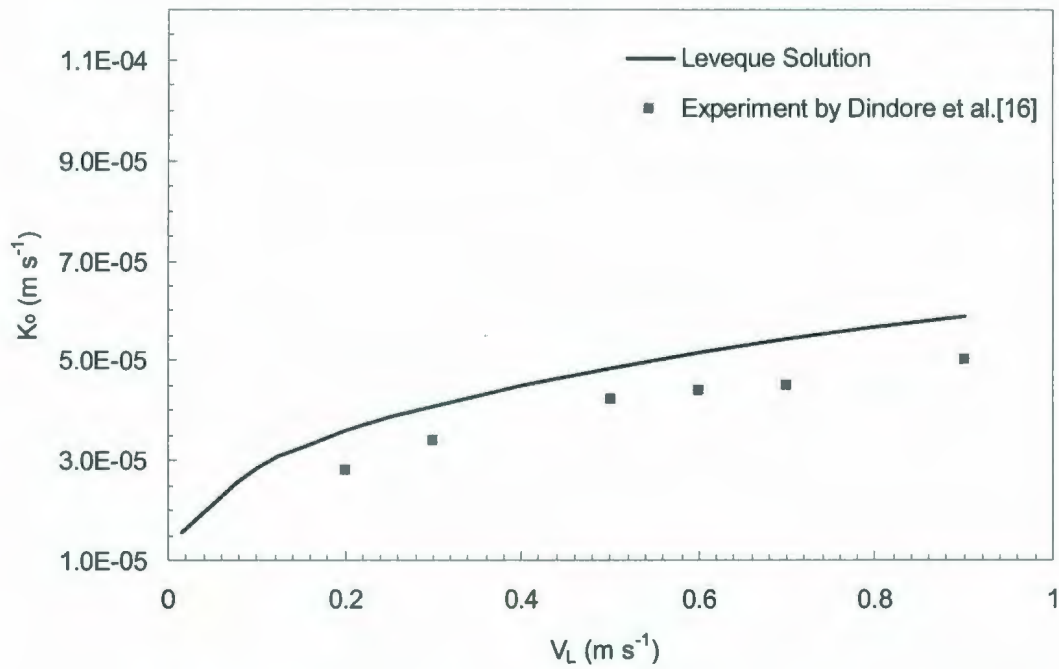


Figure 4.2 Mass transfer coefficients in Polypropylene hollow fiber membrane contactor

4.2.2 Comparison of Model Predictions and Experiment Measurements

In this work, CO_2 is selected as the sample contaminant in the feed gas of $\text{CO}_2\text{-CH}_4$ mixture and pure water as the absorbing liquid. Numerical model predictions for absorption of $14.62 \text{ mol/m}^3 \text{ CO}_2$ at constant inlet gas flow rate of $2.21 \times 10^{-4} \text{ m}^3/\text{s}$ was compared to experiments [16]. To simplify the model, the liquid flow rate in the module was assumed to be constant during the absorption process and the impact of flow rate on absorption efficiency is discussed in the following chapter.

The CO₂ concentration change in both water and mixture gas phase are shown in Figure 4.3 and 4.4. As the liquid flow rates increases, the CO₂ concentration in gas outlet decreases as well as that in liquid outlet, which confirms that the mass transfer resistance is in the liquid side. The model predictions of both gas and liquid outlet concentration are in good agreement with experiments [16].

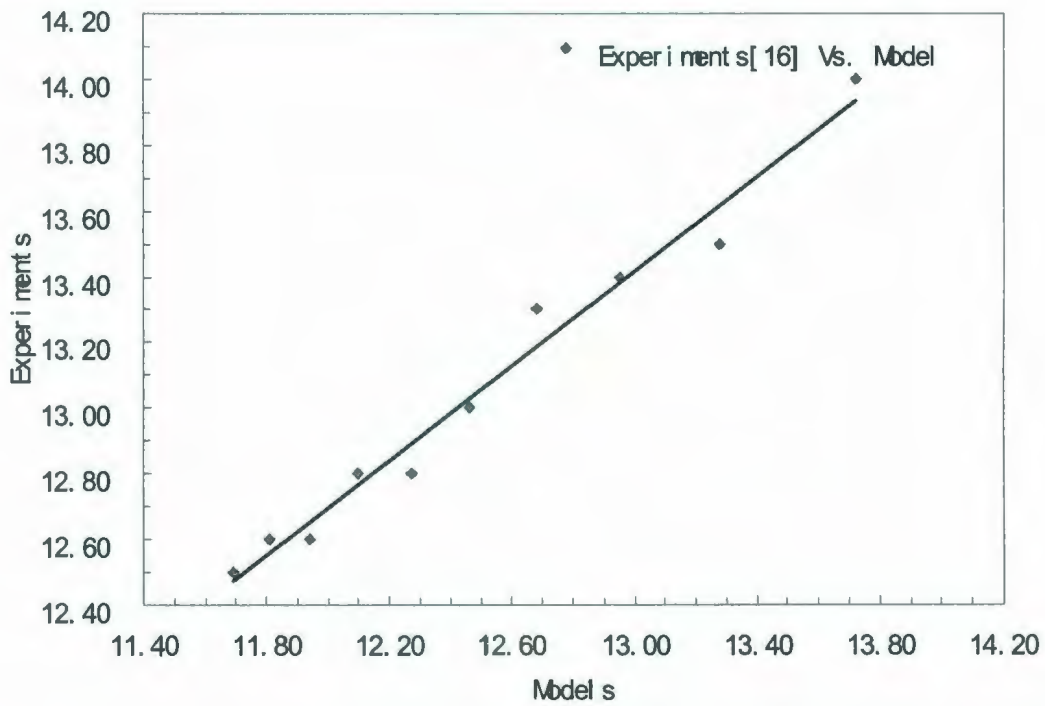


Figure 4.3 CO₂ concentration profile at gas outlet under different liquid flow rate for constant inlet gas flow rate of $2.21 \times 10^{-4} \text{ m}^3/\text{s}$ and inlet gas concentration of 14.62 mol/m^3

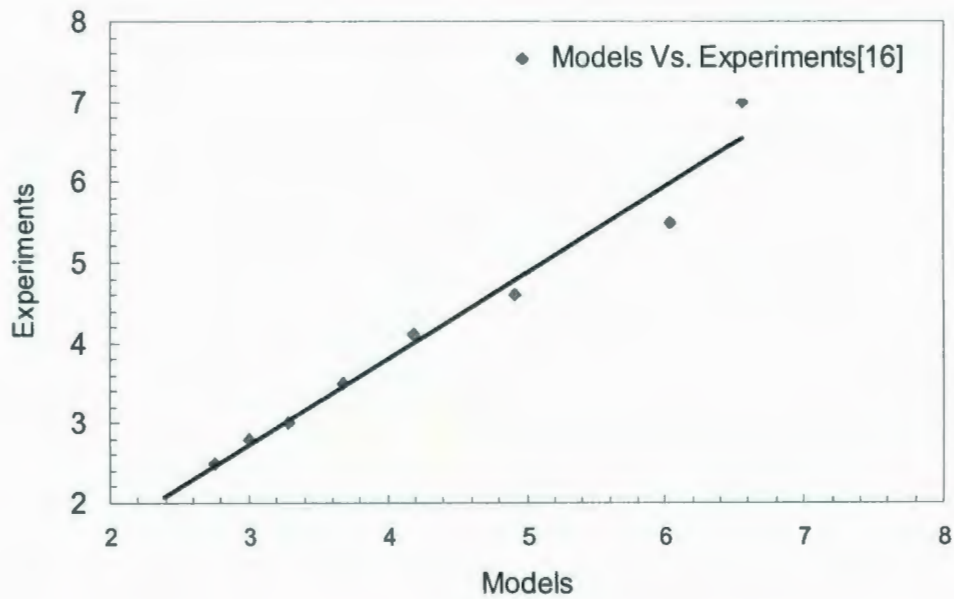


Figure 4.4 CO₂ concentration profile at liquid outlet under different liquid flow rate for constant inlet gas flow rate of $2.21 \times 10^{-4} \text{ m}^3/\text{s}$ and inlet gas concentration of 14.62 mol/m^3

4.3 Dual Membrane Module I

In Module I, nonporous membrane fibers are introduced into the single HFMC with low pressure or vacuum inside the fibers. For HFMC with the liquid flows on the tube side, the pressure drop inside the tube may lead to membrane wetting quickly in the initial fiber length due to a higher trans-membrane pressure in this section than the breakthrough pressure [25]. Considering that the diffusion of a gaseous species in the liquid phase is much slower than in the gas phase, the membrane resistance can increase significantly if it operates in the wetted mode, as such, in our module, the

liquid flows in the shell side of HFMC. Parameters used in calculation are shown in

Table 4.2:

Table 4.2 Parameters in the numerical model

Parameter	Value
Module Height (m)	0.2
Dimension of module (m)	0.1×0.1
H ₂ O flow rate (10 ⁻⁴ m ³ /s)	1.74
Mixture gas flow rate (10 ⁻⁴ m ³ /s)	2.66
CO ₂ inlet concentration (mol/m ³)	39.33
Diffusivity of CO ₂ in H ₂ O (10 ⁻⁹ m ² /s)	1.8
Pressure of mixture gas (10 ⁶ PaA)	5.0
Pressure in nonporous fibers (10 ⁵ PaA)	1.0
Number of non porous fibers	4,900
Number of porous fibers	4,900

4.3.1 Mass Transfer correlation on shell side

For a liquid flowing across a bundle of hollow fibers, the outside fiber diameter can be used as the characteristic length [4]. Taking into account the outside fiber diameter, d_{out} , and the physical properties of the liquid phase, the dimensionless numbers for the shell side are defined as:

$$Sh = \frac{k_L d_{out}}{D}$$

$$Re = \frac{d_{out} V}{\nu}$$

$$Sc = \frac{\nu}{D}$$

where, D is the diffusion coefficient of the gas in the liquid (here CO_2 in water). The velocity is hard to define due to the geometry of the modules and as the superficial velocity is defined as the liquid volumetric flow rate divided by the cross-sectional area for flow.

4.3.2 Absorption Performance under Constant Flow Velocity

The performance of Module I with an inlet concentration of $39.33 \text{ mol/m}^3 \text{ CO}_2$ at constant inlet gas flow rate of $2.66 \times 10^{-4} \text{ m}^3/\text{s}$ and liquid flow rate of $1.74 \times 10^{-4} \text{ m}^3/\text{s}$ is shown in Figure 4.5.

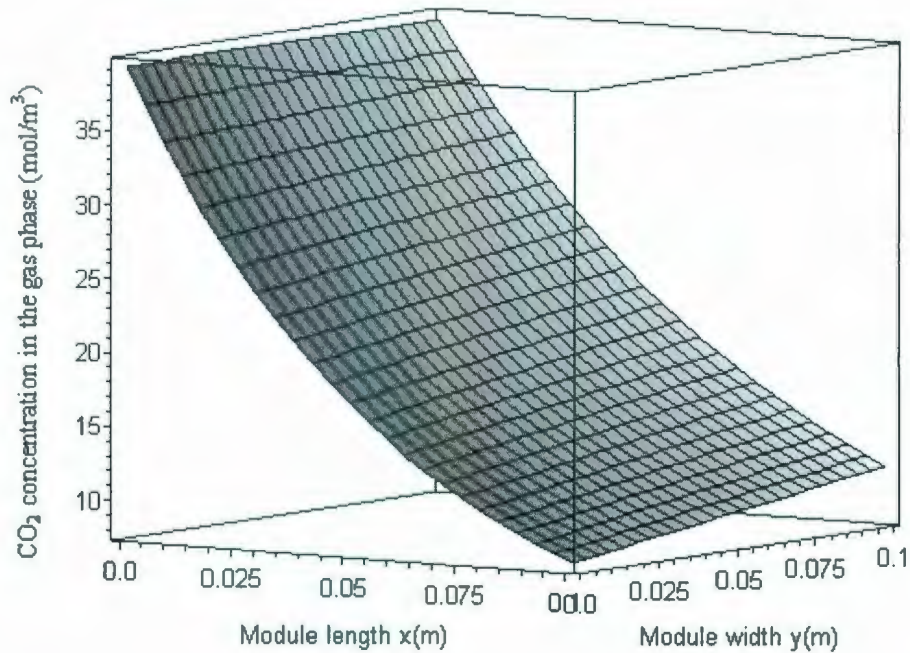


Figure 4.5 Fiber-side concentration profile of 39.33 mol/m^3 inlet CO_2 in Module I for constant inlet gas flow rate of $2.66 \times 10^{-4} \text{ m}^3/\text{s}$ and liquid flow rate of $1.74 \times 10^{-4} \text{ m}^3/\text{s}$

When constant inlet gas flow rate is $2.66 \times 10^{-4} \text{ m}^3/\text{s}$, most of the CO_2 is removed from the gas phase. It can be seen from Fig. 4.5 that the drop in the shell-side solute concentration in the direction of gas flow is very sharp at the water entrance as compared to the water exit. This is because the driving force is the largest in the module where mixture gas first meets the clean unloaded liquid. However, at the water exit, the water is partially loaded with the CO_2 and hence the decrease in the shell-side CO_2 concentration near the water exit is smaller. The combination of these effects results into reversal of the concentration driving force gradient along the length of fiber near the gas exit. The shell-side concentration profile is also useful in

identifying less efficient zone for mass transfer. The region near the water entrance and the gas exit has very low gas concentration and therefore is less efficient in the mass transfer process. In such cases, the installation of baffles perpendicular to gas flow to enhance the mass transfer in these zones will improve the overall driving force. The CO₂ concentration profile along the membrane length in liquid phase and the nonporous fibers are shown in Figure 4.6.

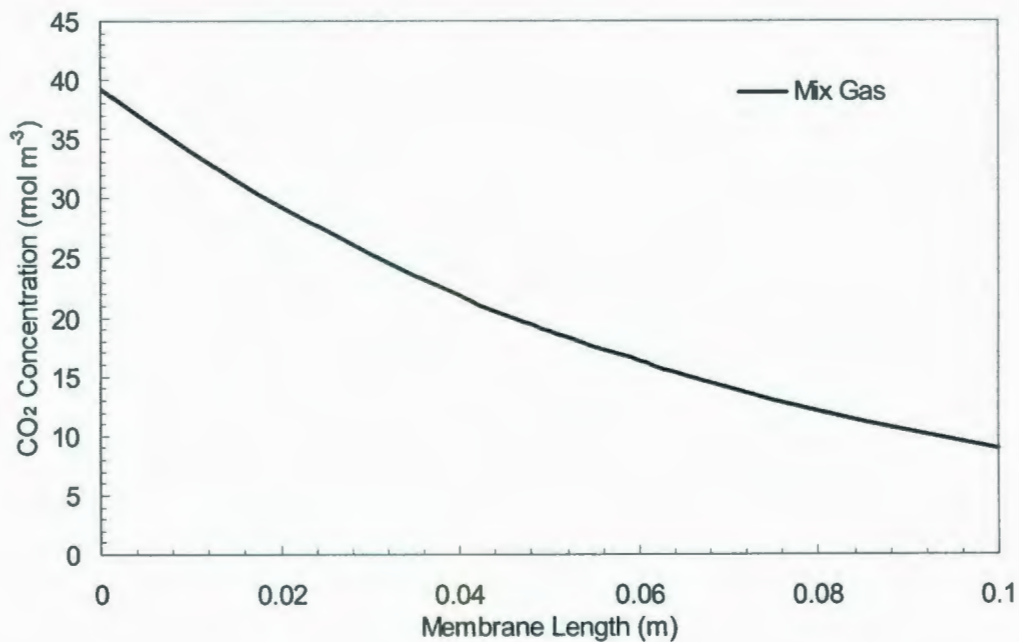


Figure 4.6 Fiber side concentration profile of 39.33 mol/m³ CO₂ in Module I for constant inlet gas flow rate of 2.66x10⁻⁴ m³/s and liquid flow rate of 1.74x10⁻⁴ m³/s

It shows in Figure 4.6 that the CO₂ concentrations in both porous fibers and nonporous fibers decrease with the membrane length. In cross flow mode, when liquid first meets gas at gas inlet, the fresh liquid has a best potential to absorb CO₂ though the absorbing ability decreases as the liquid is gradually loaded along the membrane

length, thereby, the CO₂ concentration in nonporous membrane decreases with the decrease of CO₂ in the liquid side due to less concentration gradient between the nonporous membranes. On the shell side where liquid passes through, the CO₂ concentration increases along the membrane width as shown in Figure 4.7 which is mainly due to longer gas and liquid contact time.

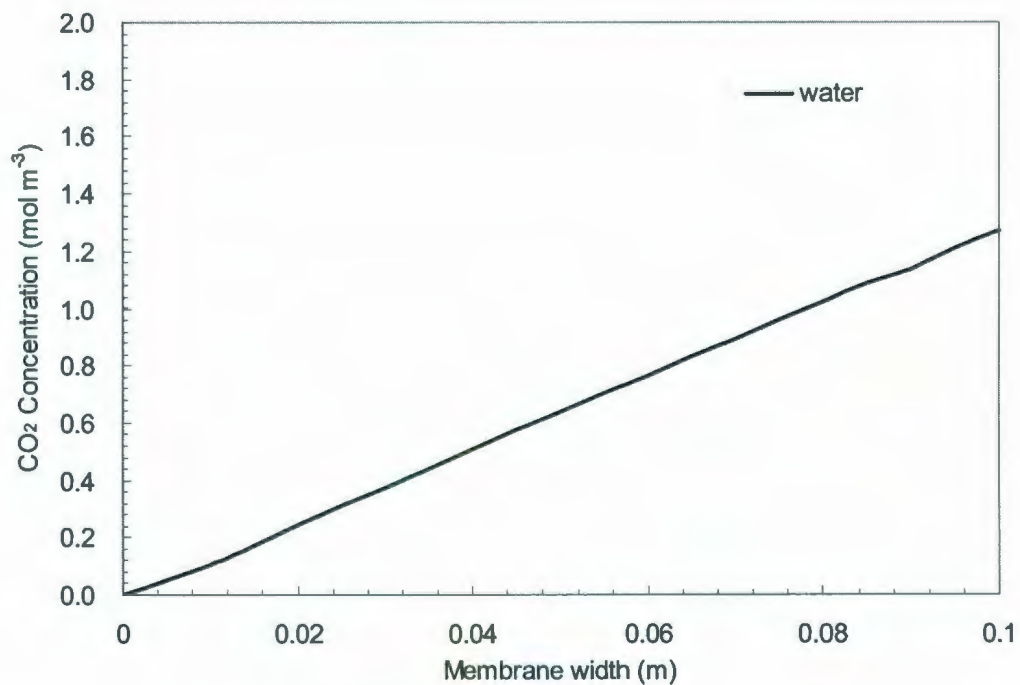


Figure 4.7 Shell side concentration profile of 39.33 mol/m³ CO₂ in Module I for constant inlet gas flow rate of 2.66x10⁻⁴ m³/s and liquid flow rate of 1.74x10⁻⁴ m³/s

Table 4.3 shows the CO₂ concentration variation in shell and liquid sides, the CO₂ concentration in the mixture gas decreases from 39.33mol/m³ to 8.906mol/m³ while the concentration in the nonporous membrane increases from 0 to 4.03mol/m³ and the concentration in the solvent increases from 0 to 1.29mol/m³. The absorption efficiency

of CO₂ in Module I is 77.2%

Table 4.3 CO₂ inlet and outlet concentration in Module I

CO ₂ Concentration	C_{in} (mol/m ³)	C_{out} (mol/m ³)
Mixture gas	39.33	8.96
Solvent	0	1.29
Nonporous membrane	0	4.03

4.4 Dual Membrane Module II

In Module II, two baffles are introduced into the dual module, evenly dividing the module into three segments, as shown in Figure 3.3. The baffles are 0.075m in length with the first one is upward and the other is downward. The liquid enters the first segment and flows across the bundle of fibers and then enters into the second segment. By subdividing the area for flow, both types of baffles increase the velocity of the shell fluid and lead to improved mass transfer. In addition, the baffles can also provide physical support for the fibers. The impacts of different baffles in module performances are discussed in Chapter 5.

4.4.1 Absorption Performance under Constant Flow velocity

Absorption of 39.33 mol/m^3 CO_2 for constant inlet gas flow rate of $2.66 \times 10^{-4} \text{ m}^3/\text{s}$ and liquid flow rate of $1.73 \times 10^{-4} \text{ m}^3/\text{s}$ was carried out to study the performance of dual membrane Module II. The numerical model predictions of CO_2 are shown in Figure 4.8:

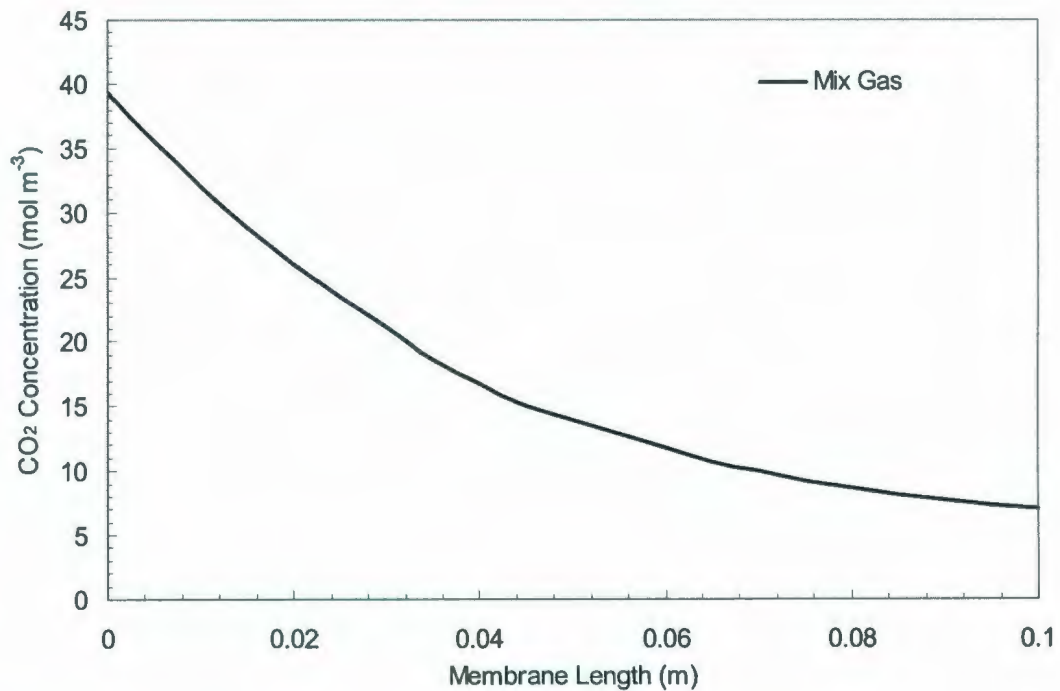


Figure 4.8 Concentration profile of 39.33 mol/m^3 CO_2 in Module II for constant inlet gas flow rate of $2.66 \times 10^{-4} \text{ m}^3/\text{s}$ and liquid flow rate of $1.74 \times 10^{-4} \text{ m}^3/\text{s}$

Similar to the module I, the CO_2 concentrations in both porous fibers and nonporous fibers decrease along the membrane length. The liquid changes direction at upside of each baffle and meets mix gas with relatively lower concentration, which results in

less CO₂ diffuse through the porous membrane.

The CO₂ concentration in the mixture gas decreases from 39.33 mol/m³ to 6.99 mol/m³ whereas the CO₂ concentration in the solvent increases from 0 to 3.46 mol/m³ and the CO₂ concentration in the nonporous membrane increase from 0 mol/m³ to 6.22 mol/m³, as shown in Table 4.4. The CO₂ absorption efficiency in Module II is 82.2%

Table 4.4 CO₂ inlet and outlet concentration in Module II

CO ₂ Concentration	C _{in} (mol/m ³)	C _{out} (mol/m ³)
Mixture gas	39.33	6.99
Solvent	0	3.46
Nonporous Membrane	0	6.2

4.5 Ordinary Membrane Contactor

Same modeling was carried out in ordinary single membrane HFMC to compare the absorption performance to dual modules. Absorption of 39.33mol/m³ CO₂ for constant inlet gas flow rate of 2.66×10⁻⁴ m³/s and liquid flow rate of 1.73×10⁻⁴ m³/s was studied in the module. The CO₂ concentration profile in tube side is shown in Figure 4.9:

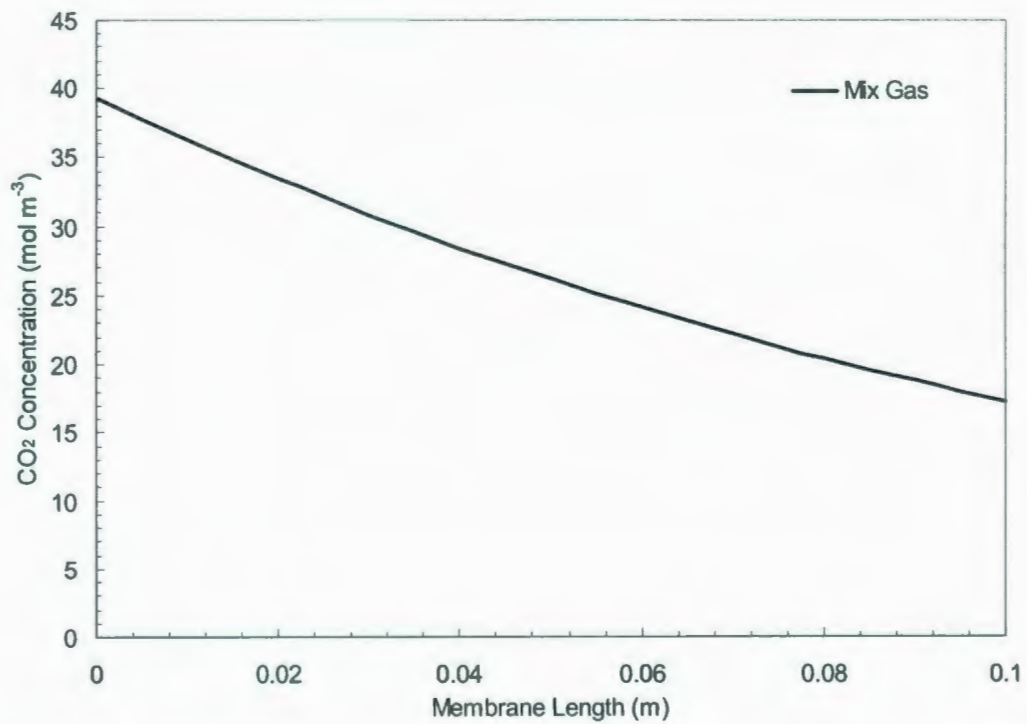


Figure 4.9 Fiber side concentration profile of 39.33mol/m^3 in ordinary membrane contactor for constant inlet gas flow rate of $2.66 \times 10^{-4}\text{m}^3/\text{s}$ and liquid flow rate of $1.74 \times 10^{-4}\text{m}^3/\text{s}$

Similar to the dual membrane modules, the CO₂ concentration of ordinary single membrane HFMC in the fiber side decreases along the length of membrane though the concentration in the shell side increases along the membrane width, shown in Figure 4.10.

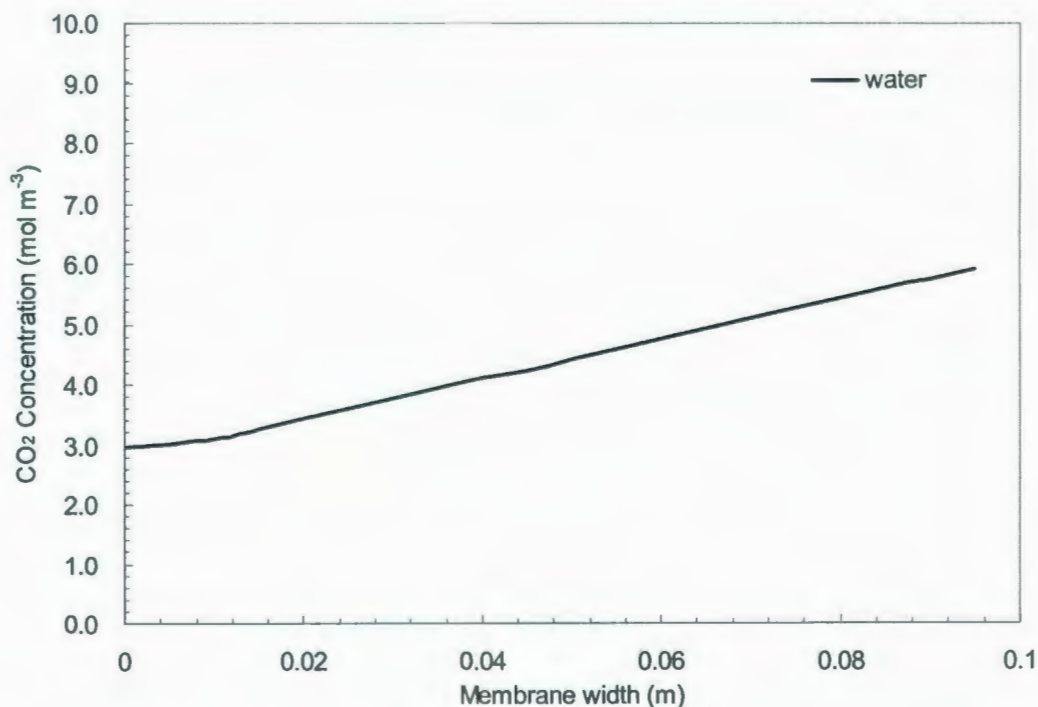


Figure 4.10 Shell side concentration profile of 39.33 mol/m^3 CO_2 in ordinary membrane contactor for constant inlet gas flow rate of $2.66 \times 10^{-4} \text{ m}^3/\text{s}$ and liquid flow rate of $1.74 \times 10^{-4} \text{ m}^3/\text{s}$

Table 4.5 shows the CO_2 concentration change in shell side and fiber side of ordinary membrane contactor. CO_2 concentration in mixture gas decreases from 39.33 mol/m^3 to 17.24 mol/m^3 along the membrane length and the CO_2 concentration in solvent increases from 0 to 7.27 mol/m^3 . The CO_2 absorption efficiency is 56%. It is clear that the CO_2 concentrations at both liquid and gas outlet are higher than dual hollow fiber module due to missing of nonporous hollow fibers as stripping system.

Table 4.5 CO₂ inlet and outlet concentration in ordinary membrane HFMC

CO ₂ Concentration	$C_{in}(\text{mol/m}^3)$	$C_{out}(\text{mol/m}^3)$
Mixture gas	39.33	17.24
Solvent	0	5.92

4.6 Comparison of Module Performances

Figure 4.8 compares the CO₂ concentration profiles in mixture gas in Module 1, Module II and ordinary membrane contactor. Absorption of 39.33 mol/m³ CO₂ at constant solvent flow rate of 1.73x10⁻⁴ m³/s and gas flow rate of 2.66x10⁻⁵ m³/s. Both Modules I and II show advantages over the ordinary single HFMC. Low press in the nonporous membrane could can partially regenerate the solvent during the absorption and result in a better gas removal efficiency. As shown in the Figure, the dual HFMC contactors can improve CO₂ removal performance by 25% compared to the ordinary membrane contactor under the same solvent flow rate. Moreover, the appearance of baffles in the Module can improve CO₂ removal performance to 10% (when the baffle number is 2) compared to dual membrane Module I. The CO₂ concentrations at gas outlet in three modules are listed in Table 4.6.

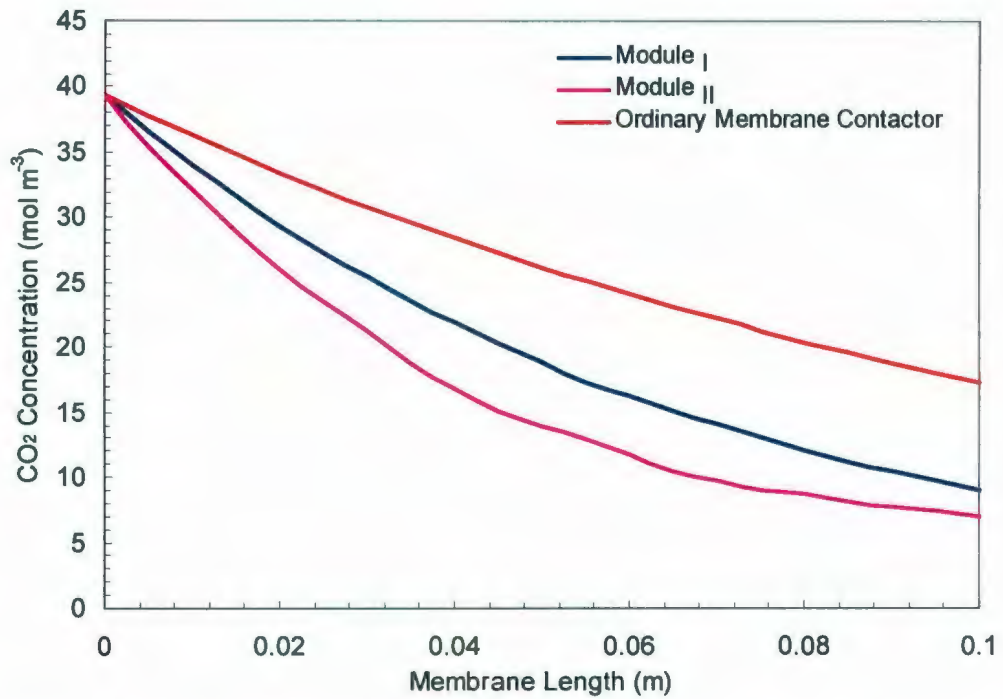


Figure 4.11 CO₂ concentration profiles of mixture gas in different Modules for constant inlet gas flow rate of $2.66 \times 10^{-4} \text{ m}^3/\text{s}$ and liquid flow rate of $1.74 \times 10^{-4} \text{ m}^3/\text{s}$

Table 4.6 CO₂ concentration changes of mix gas in Module I, II and ordinary HFMC

CO ₂ Concentration in Solvent	$C_{in}(\text{mol}/\text{m}^3)$	$C_{out}(\text{mol}/\text{m}^3)$
Module I	39.33	8.96
Module II	39.33	6.99
Ordinary Membrane Contactor	39.33	17.24

The impact of the baffles numbers on the removal efficiency were discussed in Chapter 5. Table 4.7 compares the CO₂ concentration change in liquid phase of three modules for constant inlet gas flow rate of $2.66 \times 10^{-4} \text{ m}^3/\text{s}$ and liquid flow rate of $1.74 \times 10^{-4} \text{ m}^3/\text{s}$. The CO₂ concentrations at liquid outlet in the solvent from

dual-membrane contactors are lower than that from the ordinary single-membrane contactor. Meanwhile, Module II has a higher outlet CO₂ concentration comparing to Module I mainly due to the appearance of baffles, which prolongs the liquid pass and increases the gas liquid contact time. Compared to ordinary membrane contactor, CO₂ absorption efficiency in Module I is improved by 21% and that in Module II is improved by 30%

Table 4.7 CO₂ concentration change in shell side of Module I, II and ordinary HFMC

CO ₂ Concentration in Solvent	$C_{in}(\text{mol/m}^3)$	$C_{out}(\text{mol/m}^3)$
Module I	0	1.29
Module II	0	3.65
Ordinary Membrane Contactor	0	5.92

Table 4.8 compares the CO₂ concentration change in nonporous membrane in Module I and II under the same flow rates. The CO₂ concentration in nonporous fibers increases from 0 to 4.03mole/m³ in Module I whereas increases from 0 to 6.2mole/m³ in Module II. Module II seems preferable to Module I in terms of outlet CO₂ concentration in mixture gas and but received higher concentration in solvent phase. The installation of baffles in the module physically increase the path of the liquid flowing through the module which meanwhile prolongs contact time between gas and liquid, hence results in good chance of liquid to be loaded more than that in Module I.

Moreover, the baffles in real case would play the part as mechanical support of fibers, especially when shell side flow passes the fibers in a high flow rate.

Table 4.8 CO₂ concentration change in Nonporous fibres of Module I and II

CO ₂ Concentration in Nonporous Fibers	$C_{in}(\text{mol/m}^3)$	$C_{out}(\text{mol/m}^3)$
Module I	0	4.03
Module II	0	6.2

4.7 Fluid Dynamics in Module II

The baffles in Module II can not only minimize the liquid bypass but also impact on the liquid velocity, moreover, the flux and also mass transfer coefficient is a strong function of liquid flow rate, which may justify the study of fluid dynamics in shell side. As described in Chapter 3, FLUENT v.6 was used as the CFD simulation package in this work to predict velocity profiles in the shell side. Computations were performed on a grid that was generated using the meshing software GAMBIT[®] 2.2. Structured meshing was performed to divide the flow domain into 39,530 quadrilaterals cells and grid refinement was performed to achieve grid independency.

CO₂ absorption for inlet gas flow rate of $2.66 \times 10^{-4} \text{ m}^3/\text{s}$ and liquid flow rate of $1.74 \times 10^{-4} \text{ m}^3/\text{s}$ was studied. The superficial velocity at the liquid inlet is assumed to be constant, which was calculated by dividing the flow rate with superficial area at liquid

inlet as the inlet velocity. The result shows in the Figure A.1 and Figure A.2 in Appendix that the velocity magnitude has different contours and velocity changes greatly especially when liquid flows through the baffles. The maximum velocity reaches 0.1 m/s whereas the minimum is 0.

As demonstrated before, the mass transfer is a strong function of liquid flow rate. To combine the fluid dynamics of liquid in shell side with mass transfer in the module, the velocity data were exported from FLUENT and equations were fit to the velocity data. Due to the complexity of the module geometry, it is hard to conclude one function describing the velocity profile so the computational domain can be divided into several parts where fitting functions were developed for each cell, respectively. Functions fitting to the velocity values were generated by Table Curve 3D® (Function fitting software) for each cell.

The velocity functions of velocity and locations were substituted into the governing equation of mass transfer. The absorption for constant inlet gas flow rate of 2.66×10^{-4} m³/s and liquid flow rate of 1.74×10^{-4} m³/s is studied where CO₂ at gas inlet is 39.33 mol/m³. The CO₂ absorption in Module II with assumed constant velocity in liquid is compared to that with the real velocity in Table 4.9.

Table 4.9 CO₂ concentration at gas outlet in Module II with different velocity profiles

CO ₂ Concentration	C_{in} (mol/m ³)	C_{out} (mol/m ³)
Module II(constant velocity)	39.33	6.99
Module II(real velocity)	39.33	5.58

CO₂ concentration at gas outlet in Module II with constant profile decreases from 39.33mol/m³ to 6.99mol/m³, the other one with real velocity profile decreases to 5.58mol/m³. It shows that module II with simulated velocity profile receives better absorption performance which also proves that the mass transfer is a strong function of liquid velocity and the fluid dynamics should be considered in the HFMC absorption.

Chapter 5

Analysis of Model Parameters

In addition to gas composition and absorbing solvent, the absorption efficiency of HFMC also depends on the variety of model parameters such as geometry of module, solvent flow rate, gas flow rate and the pressure applied on the permeate side. In this chapter, the effects of some of the parameters on the efficiency of CO₂ removal are examined. As demonstrated in Chapter 2, both Modules I and II can improve the CO₂ removal efficiency compared to the ordinary HFMC. We focus on Module I in the analysis of parameters. The impacts of each parameter on the gas removal performance can be observed and compared by changing these parameters separately, which can subsequently lead to the optimal module design and selection of parameters in the future follow-up experiments. The common parameters are kept the same as those used in previous chapters in the following chapter.

5.1 Module Length

To examine the impact of module length on the CO₂ removal performance, modules with different lengths are studied under the same gas flow rate and liquid flow rate. The CO₂ absorption of gas phase in different modules is shown in Figure 5.1. The length differs from 0.02m to 0.2m with gas flow rate of $2.66 \times 10^{-5} \text{ m}^3/\text{s}$ and liquid flow rate of $1.73 \times 10^{-4} \text{ m}^3/\text{s}$.

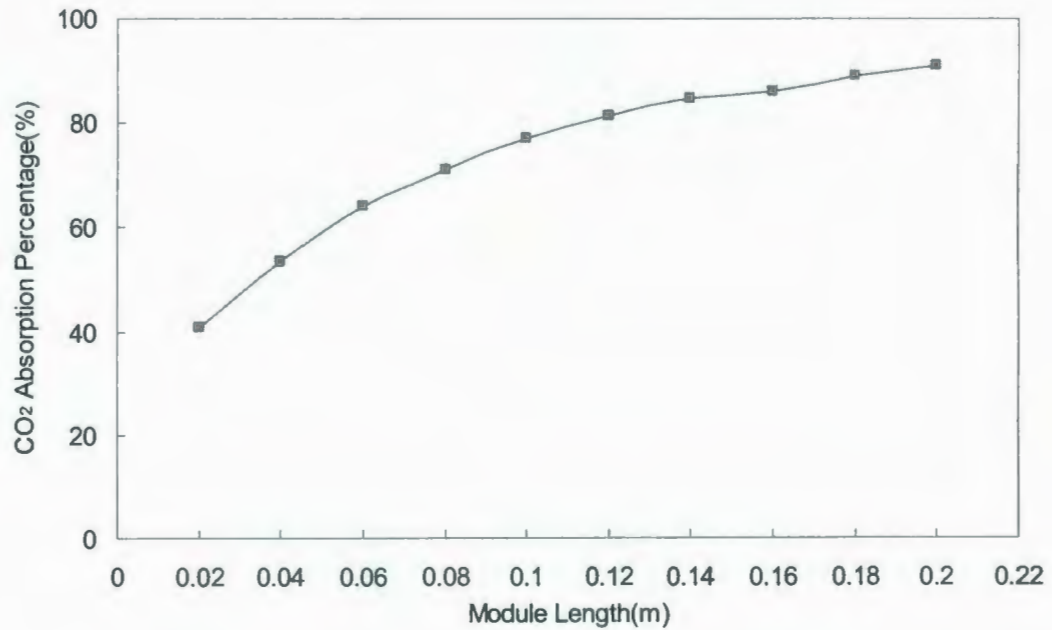


Figure 5.1 The effect of module length on CO₂ removal

As module length increases from 0.02m to 0.22m, the CO₂ absorption efficiency increases from 41% to 91%. Under the same liquid flow rate, the liquid velocity in the module with longer length is much higher, which consequently results in a better mass transfer between gas and liquid phase.

5.2 Solvent Flow Rate

As demonstrated in previous chapters, the overall mass transfer resistance mainly relies on the liquid side in non wetted liquid and gas membrane contactors, so the absorption efficiency changes as different liquid flow rates. Absorption percentage of CO₂ was compared under various volume flow rates from $1.73 \times 10^{-5} \text{ m}^3/\text{s}$ to 2.17×10^{-4}

m^3/s to examine how liquid flow rates effect the absorption performances.

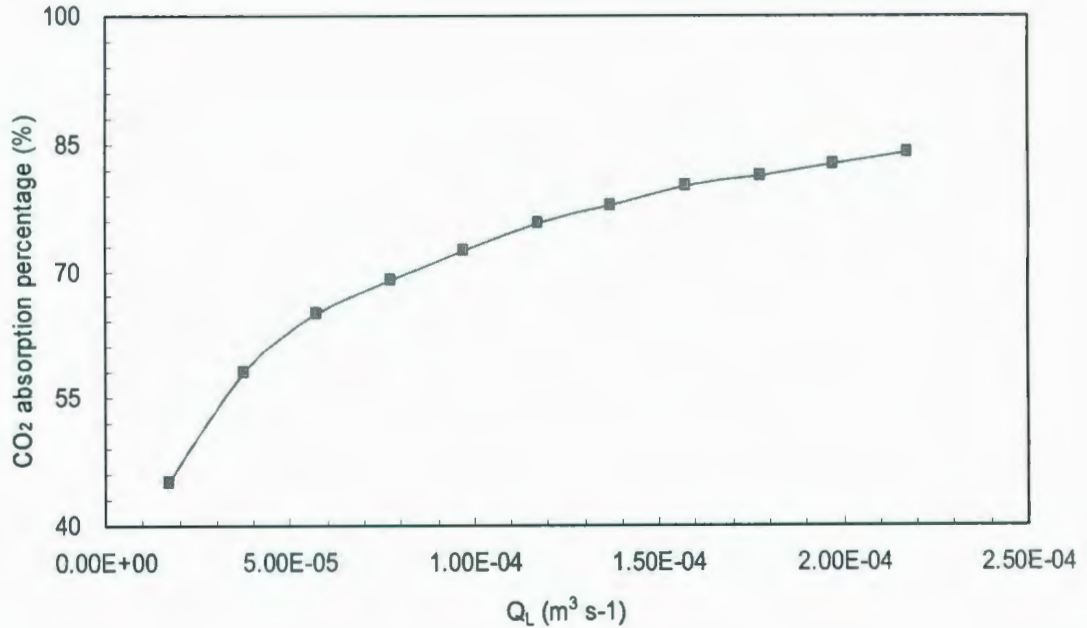


Figure 5.2 The effect of solvent flow rate on CO₂ removal

As liquid flow rate increases to 0.01 m/s, the absorption efficiency has been improved from 42% to 85%. This is due to the decreased resistance in the liquid side due to increased liquid regeneration. Moreover, at larger liquid flow rate, the liquid loaded with CO₂ is substituted quickly with fresh liquid which generates greater driving force for mass transfer between the membranes. It also confirms that in the case of physical absorption of a sparingly soluble gas, the controlling mass transfer resistance lies on the liquid side. This is a very important factor when enhanced solvents formulated for CO₂ gas removal purposes are considered in combination with a

compact membrane contactor for gas processing facilities.

5.3 Gas Flow Rate

The impact of inlet gas flow rate on the CO₂ absorption is depicted in Figure 5.3. Inlet gas flow rate is varied from 1×10^{-6} m³/s to 5×10^{-5} m³/s. It is clear from the figure that the CO₂ absorption efficiency decreases by 40% as the gas flow rate increases by a factor of five. This tendency is mainly due to less gas residence time in the module instead of mass transfer resistance which is different from the impact of liquid flow rate.

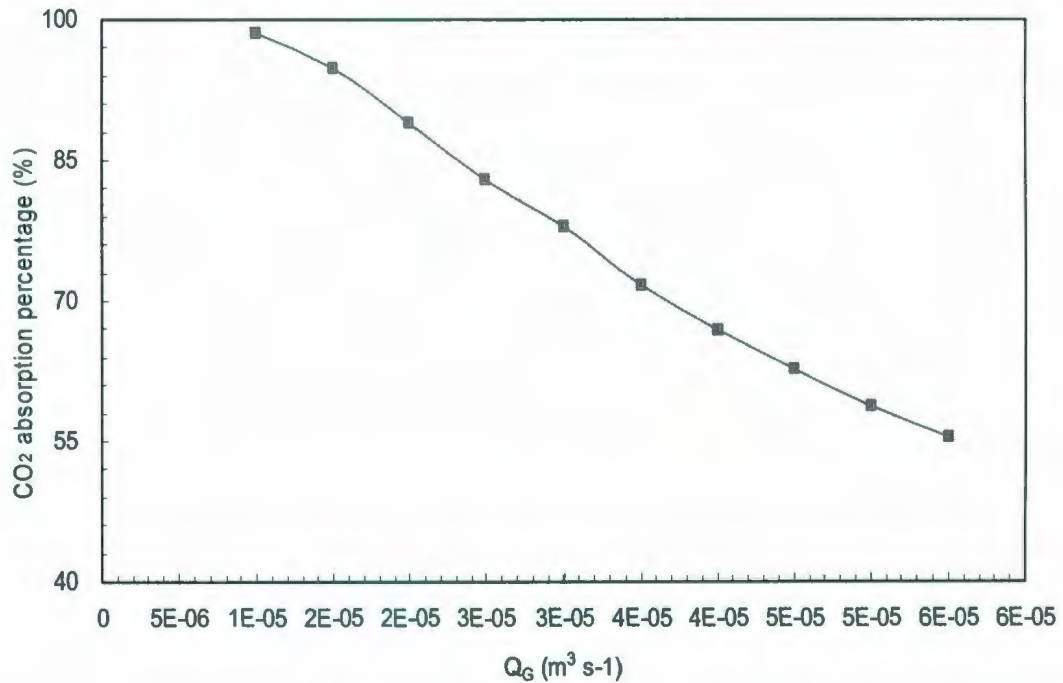


Figure 5.3 The effect of gas flow rate on CO₂ removal

5.4 Pressure on the Permeate Side

To examine the effect of the permeate side pressure on the CO₂ removal efficiency, the pressure is increased in 0.5×10^5 Pa increments starting from vacuum 0.1×10^5 Pa through 1.0×10^6 Pa.

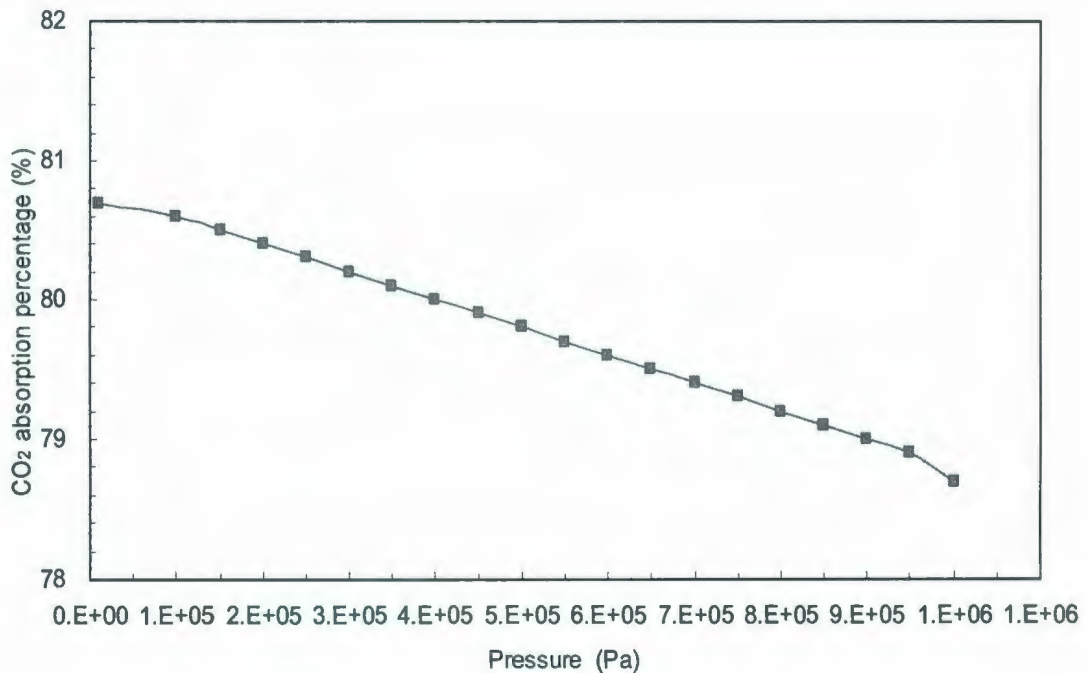


Figure 5.4 The effect of pressure on permeate side on CO₂ gas removal

From Figure 5.4 the CO₂ absorption percentage decreases from 80.7% to 78 %, almost linearly with pressure. This indicates that the lower the permeate side pressure, the better removal performance for the novel dual-membrane contactor and the highest removal percentage happens when vacuum is provided in the nonporous membrane. Considering the gas pressure in practical operation, the novel dual-membrane system can improve the performance of membrane contactors only when a positive

differential pressure exists between the solvent side and the permeate side, which the requirement for all mass transfer devices. Inversely, the mass transfer will reverse and the second membrane will impose a negative effect on the gas removal efficiency if this negative driving force happens.

5.5 The Henry's Constant

It is known that the Henry's constant is a parameter related to gas solubility and depends on the type of solvent chosen for gas treating processes. It is also known that when the solvent is changed both the Henry's constant and diffusivity will change. However, to examine the effect of Henry's constant on CO₂ removal performance, all the other parameters are kept constant and the Henry's constant is increased from 1.0 to 4.0. By comparing the CO₂ absorption efficiency under different Henry's constant values, the impact of Henry's constant can be assessed. As shown in Figure 5.5, CO₂ absorption efficiency shows an increasing trend as the Henry's constant value increases. This correlation would be helpful in solvent selection during future module construction.

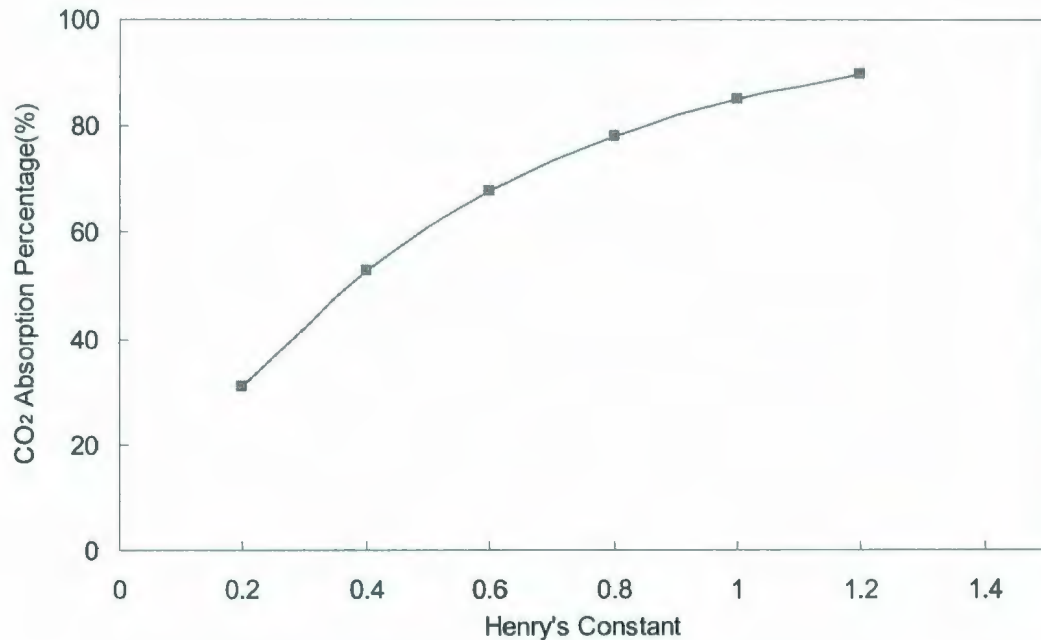


Figure 5.5 The effect of Henry's constant on CO₂ removal

5.6 Diffusion coefficient

Similar to the Henry's constant, the ability of CO₂ component diffusing through solvents varies as different combination of gas component and absorption solvent. To examine the effect of diffusivity, all the other parameters are kept constant and the diffusivity coefficient changes from $1.0 \times 10^{-9} \text{m}^2/\text{s}$ to $4.50 \times 10^{-9} \text{m}^2/\text{s}$. The CO₂ absorption efficiencies of modules with different diffusivity coefficient are shown in Figure 5.6. CO₂ absorption efficiency shows an increasing trend as the diffusivity coefficient increases which is mainly due to large rate of mass transfer between gas and liquid phase. Particular attention should be given to this issue in absorption of

different CO₂ components.

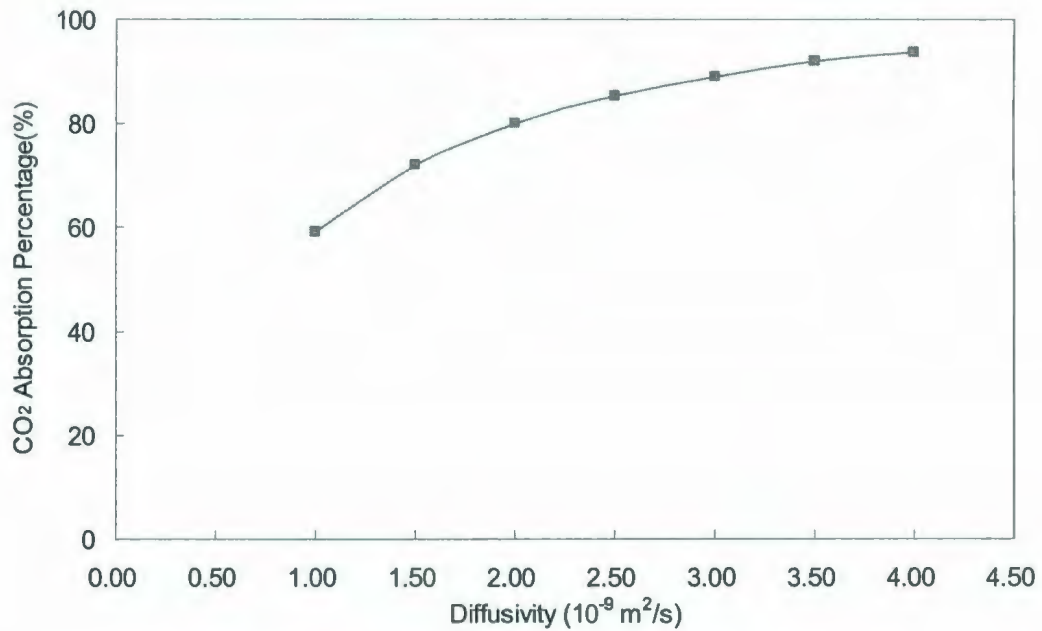


Figure 5.6 The effect of diffusivity coefficient on CO₂ gas removal

5.7 Number of Baffles

To study the effects of baffles in the module, the absorption efficiency of modules with different number of baffles has been compared. The baffle number is varied from 0 to 7. Figure 5.7 shows CO₂ removal percentage in gas outlet with different number of baffles. As the baffle number increases from zero to five, the absorption increases from 22% to 57%. This demonstrates the positive effect baffles have on the mass transfer by providing a velocity component normal to the membrane surface. In practical operation, the cost of complicated geometry should also be considered in although more baffles could bring higher removal efficiency.

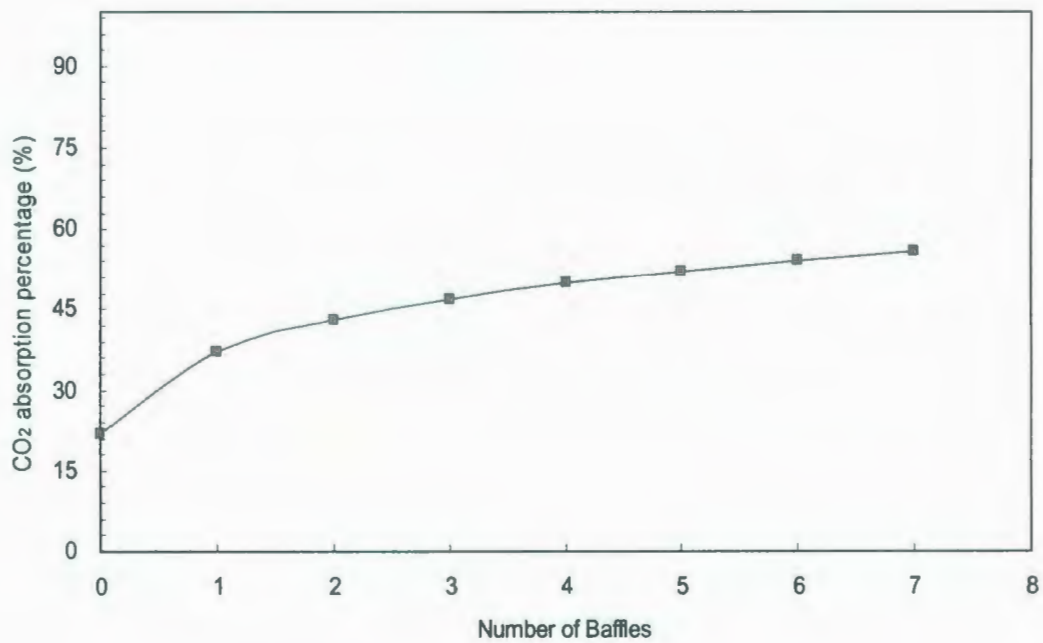


Figure 5.7 The effect of number of baffles on CO₂ removal

5.8 Permeability of nonporous fibres

The effect of the permeability of nonporous fibre on CO₂ removal has also been studied. All the other parameters are kept same and the permeability of nonporous fibres varies from 500 to 45,000 Barrer. The CO₂ absorption efficiencies slightly increase as permeability increases which shows that the nonporous membrane with higher permeability would be preferred in the dual membrane module for CO₂ removal.

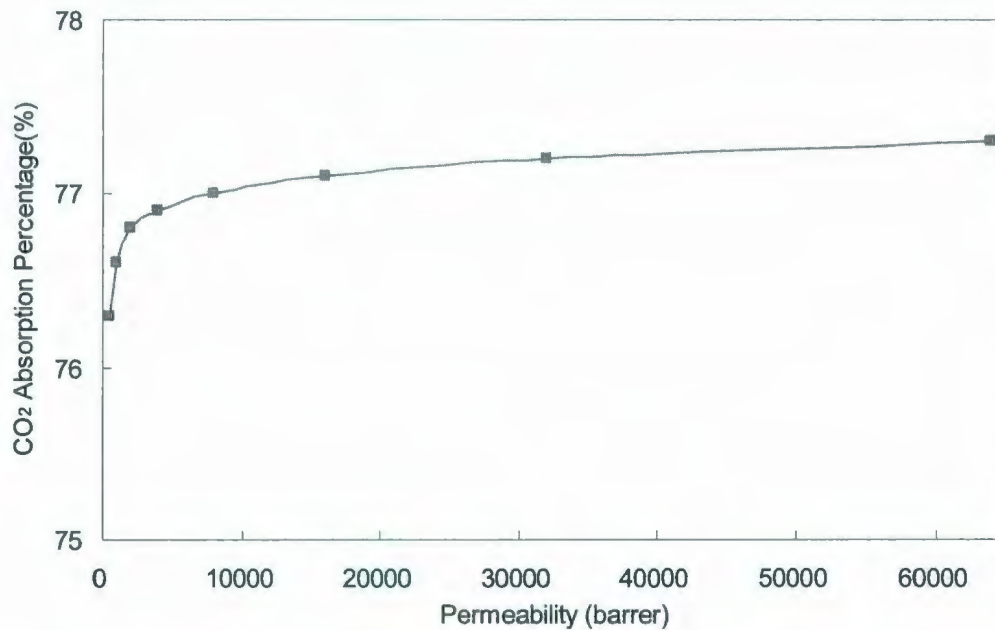


Figure 5.8 The effect of permeability of nonporous membrane on CO₂ removal

The discussions above mainly focus on the effect of individual parameters on the novel dual membrane hollow fiber systems. However, in real engineering design, certain parameters likely interact with each other, which would need to take an extensive analysis into consideration to obtain the optimum performance and economic value.

In addition, all the above analysis is based on the CO₂ and water system, so when the CO₂ component or absorption solvent changes, the optimum operating parameters will also change accordingly.

Chapter 6

Conclusions

6.1 Summary

This thesis conceptually proposes two dual-membrane configurations to improve the performance of the ordinary single-membrane HFMC. In Module I, nonporous membrane fibres are added into the module and arranged alternately with porous membrane fibres. Meanwhile, low pressure is provided on the permeate side of the nonporous fibres; In Module II, in addition to nonporous membrane fibres and low pressure, baffles are introduced, equidistantly placed along the membrane width in the module. Theoretically both modules can partially regenerate the solvent stream simultaneously with the absorption process, thereby obtaining a better efficiency. Additionally, to demonstrate the efficiency of two dual hollow fibre modules for the removal of gaseous contaminants compared to ordinary single membrane HFMC, a novel mathematical modeling approach using mass balance principles governing the absorption and stripping processes is proposed to predict absorption performances of two novel modules as well as ordinary module.

The novel numerical model is partially verified by being applied on the module proposed by Dindore *et al.* The predictions of the model are compared to experimental data [16]. The proposals of novel modules and ordinary HFMC are also modeled with

partial differential equations and solved numerically based on single-component absorption to check how the novel modules can improve the performance. Considering the impact of the shell side flow rate on the mass transfer in Module II, velocity magnitude in the module has been modeled in CFD software, the modelling results are imported into surface fitter to find idea linear equations to describe three dimensional empirical data, which can be incorporated into the numerical model to investigate the mass transfer as the velocity changes. A series of analysis was implemented based on the solutions to check how various parameters affect the CO₂ removal performance.

6.2 Conclusions

Based on the analysis and the comparisons between the proposed dual-membrane HFMC and ordinary single-membrane HFMC, it can be concluded that:

1. Both novel dual-membrane modules can substantially improve the CO₂ removal efficiency over ordinary single-membrane HFMC under suitable parameter choice and operating conditions;
2. From the engineering perspective, Module II is more efficient than Module I to improve the performance of ordinary membrane contactor but may also cost more in construction.
3. The module length poses a significant impact on the performance of both modules; the better removal performance can be expected as module length increases.

4. The permeate side pressure also plays an important role on absorption performance. The better removal performance for Module II can be expected. However, the nonporous membrane will impose a negative effect on the gas removal efficiency when the permeate side pressure is too high.
5. When Henry's constant is in a certain range, the performance of Module II would be improved as the Henry's constant increases.
6. The change in diffusivity coefficient would also impact on absorption efficiency. Improvement can be expected from the dual-membrane contactor when the diffusivity coefficient increases.
7. The large solvent flow rate can improve the solvent regeneration which is helpful for the absorption efficiency for dual membrane modules. On the contrast, the gas flow rate impacts on the opposite way. Larger gas flow rate would results in decreasing absorption efficiency due to less gas and liquid contact time.
8. The absorption efficiency shows a slight increasing trend when the permeability increase. However, when permeability is larger than a certain value, increasing permeability will not result in a significant improvement to the performance.

6.3 Follow-up work

All the analysis and predictions regarding the novel dual-membrane contactors are based on mathematical models and therefore at a conceptual stage, to verify whether and how the configurations can improve the performance realistically, an experimental

set-up should be designed and tests carried out in the following work, which will take the membrane wetting and swelling problem into consideration along with absorption process. In addition, the velocity profile in the shell side should also be extended to be compared to the model simulation. Due to the geometry complexity resulted in by the presence of fibers in the module, the velocity field studied in this work did not consider the fibers in the shell side. However the presence of fibers would definitely have a significant impact on the velocity change and probably would result in a plug flow. If the velocity change in shell side could be measured in accurately in experiments, the impact of velocity on absorption efficiency could be understood better, which will be helpful in facility design and process control for natural gas processing through HFMC.

References

- [1] R. W. Baker, K. Lokhandwala, (2008). "Natural Gas Processing with Membranes: An Overview". *Ind. Eng. Chem. Res.*, Vol. 47, no.7, pp 2109–2121
- [2] A. Gabelman, S. Hwang, (1999). "Hollow fiber membrane contactors", *J. Membr. Sci.*, Vol. 159, pp. 61-106.
- [3]. V. Y. Dindore, (2003). Ph.D. Thesis, University of Twente, The Netherlands.
- [4]. K. L. Wang, E.L. Cussler, (1993). "Baffled membrane modules made with hollow fiber fabric", *J. Membr. Sci.*, Vol. 85, pp. 265-278.
- [5]. Marcel Mulder, (1996). *Basic Principles of Membrane Technology*, Springer, The Netherlands.
- [6] H. B. Al-Saffar, B. Ozturk, R. Hughes, (1997). "A comparison of porous and non-porous gas-liquid membrane contactors for gas", *Chemical engineering research & design*, Vol. 75, no 7, pp. 633-676
- [7] Osada, Y., Nakagawa, T., *Membrane Science and Technology*, New York: Marcel Dekker, Inc, 1992
- [8] S. Karoor and K. K. Sirkar, (1993). "Gas Absorption Studies in Microporous Hollow Fiber Membrane Modules", *Industrial & Engineering Chemistry Research*, Vol. 32, pp. 674-684.
- [9] M. Mavroudi, S. P. Kaldis, G. P. Sakellariopoulou, (2003). "Reduction of CO₂ emissions by a membrane contacting process", *Fuel*, Vol. 82, pp. 2153-2159.
- [10] A. Malek, K. Li, and W. K. Teo, 1997. "Modeling of Microporous Hollow Fiber Membrane Modules Operated under Partially Wetted Conditions", *Industrial & Engineering Chemistry Research*, Vol. 36, pp. 784-793.
- [11] A. H. P. Skelland, 1974. *Diffusional Mass Transfer*, John Wiley & Sons Inc, New York.
- [12] A. L. Kohl, R. B. Nielsen, (1997). *Gas Purification*, 5th Edition; Gulf Publishing: Houston, TX,
- [13] C. T. Ratcliffe, A. Diaz, C. Nopasit, G. Munoz, (1999). "Application of membranes in CO₂ separation from natural gas: pilot plant tests on offshore platforms". *In Proc. -Laurance Reid Gas Cond. Conf.*

- [14] Z.Qi, E. L. Cussler, 1985. "Microporous Hollow Fibers for Gas Absorption: Mass Transfer Across the Membrane", *J. Membrane Sci.*, Vol. 23, pp.:333
- [15] Dindore, V. Y., and Versteeg, G.F. (2005). "Gas-liquid mass transfer in a cross-flow hollow fiber module: Analytical model and experimental validation". *International Journal of Heat and Mass Transfer*, Vol. 48, pp.:3352-3362.
- [16] Dindore, V. Y., Brillman, D. W. F., and Versteeg, G. F. (2005). "Modelling of cross-flow membrane contactors: physical mass transfer processes". *J. Membrane Sci.*, Vol.279, pp.:301-310
- [17] Wang, S. Y., Hawboldt, K., and A. Abdi, M. (2006). "Novel Dual-Membrane Gas-Liquid Contactors: Modeling and Concept Analysis". *Ind. Eng. Chem. Res.*, Vol. 45, pp.:7882-7891
- [18] Wickramasinghe, S.R., Semmens, M. J., and Cussler, E. L. (1992). "Mass transfer in various hollow fiber geometries". *J. Membrane Sci.*, Vol. 69, pp.:235-250.
- [19] Yang, M. C., and Cussler, E. L. (1986). "Hollow fiber gas treating". *AIChE J.*, Vol.32, pp.:1910-1916.
- [20] X. Jiang, A. Kumar, (2005). "Performance of silicone-coated polymeric membrane in separation of hydrocarbons and nitrogen mixtures", *J. Membrane Sci.*, Vol. 254, Iss. 1-2, pp 179-188
- [21] C. T. Blaisdell and K. Kammermeyer,(1973). "Countercurrent and cocurrent gas separation", *Chem. Eng. Sci.*, Vol.28 ,page:1249
- [22] S. A. Stern and W. P. Walawender, (1969). "Analysis of Membrane Separation Parameters", *Sep Sci.*, Vol. 4, p. 123.
- [23] H. Kreulen, C. A. Smolders, G. F. Versteeg and W. P. M. Van Swaaij,(1993). "Microporous hollow fiber membrane modules as gas-liquid contactors", *J. Membrane Sci.*, Vol. 78, p.197-238
- [24] Skelland, A. H. P. (1974). "*Diffusional Mass Transfer*". New York: John Wiley & Sons.
- [25] A.Gabelman, S. Hwang, (2006). "A theoretical study of dense gas extraction using a hollow fiber membrane contactor". *J. of Supercritical Fluids*, Vol. 37, p. 157-172.

[26] Waterloo Maple Inc.,(1998). "Maple Guide", Waterloo, CA.

[27] R. K. Shah, and D. P. Sekulic (2003). "Fundamentals of Heat Exchanger Design"
John Wiley & Sons, page 503.

[28] F. P. Incropera, D. P. DeWitt, (1990). "*Fundamentals of Heat and Mass Transfer*
(3rd ed.)", *John Wiley & Sons*. pp. p. 345.

Appendix A

A.1 Grid Generation

The baffles in Module II can not only minimize the liquid bypass but also improve the liquid velocity, moreover, the flux and also mass transfer coefficient is a strong function of liquid flow rate, which makes the study of fluid dynamics in shell side a must. As described in Chapter 3, the FLUENT v6 was used as the CFD (Computational Fluid Dynamics) simulation package in this work to visualize the change of flow rates in the shell side. Computations were performed on a grid that was generated by using the meshing software GAMBIT® 2.2. Structured meshing was performed to divide the flow domain into 39,530 quadrilaterals cells and grid refinement was performed to achieve grid independency, as shown in Figure A.1.

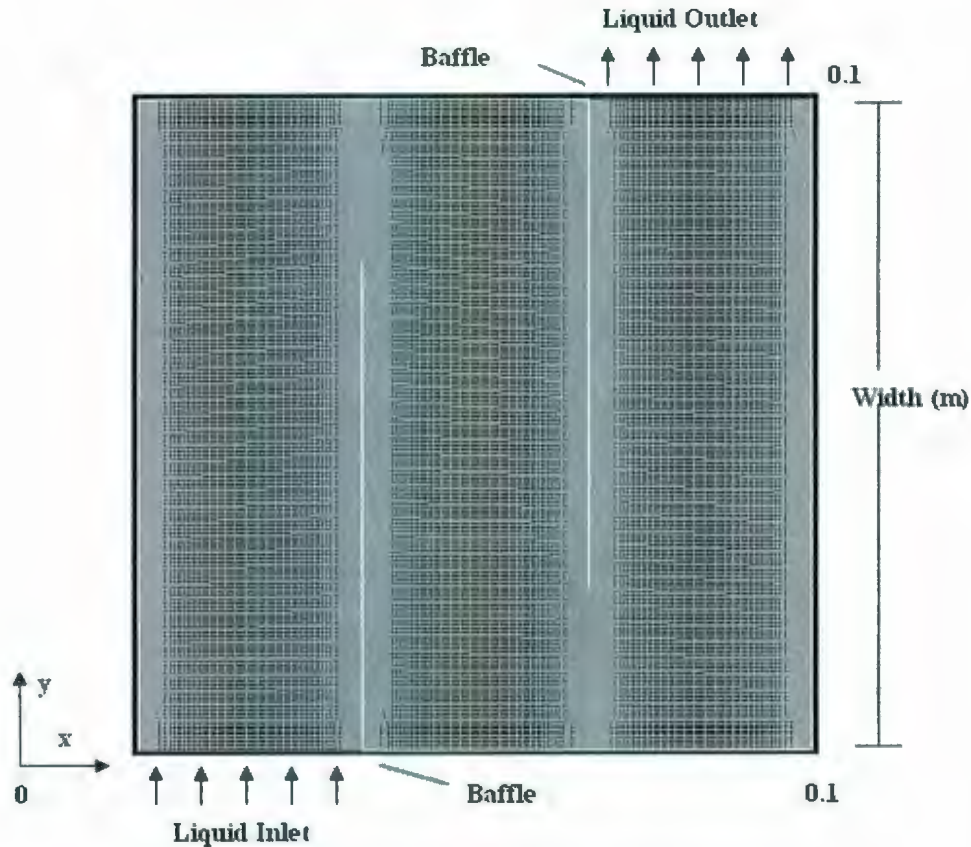


Figure A.1 Grid of flowing interior in Module II

A.2 Contours of liquid velocity magnitude in shell side of Module II

The discretized governing equations in Chapter 3 were solved in each cell based on finite volume technique. The discrete velocities and pressures were stored by a non-staggered system, which consists of cells and faces. These values were stored in the cells center. The velocity and pressure parameters would be linked and solved by SIMPLE algorithm and accelerated by algebraic multi-grid solver (AMG). CO_2 absorption for inlet gas flow rate of $2.66 \times 10^{-4} \text{ m}^3/\text{s}$ and liquid flow rate of $1.74 \times 10^{-4} \text{ m}^3/\text{s}$ was studied. The superficial velocity at the liquid inlet is assumed to be constant,

which was calculated by dividing the flow rate with superficial area at liquid inlet as the inlet velocity. Figure A.2 shows the contours of velocity change in the shell side with inlet superficial velocity is 0.025 m/s. It shows in the figure that the velocity magnitude has different contours and velocity changes greatly especially when liquid flows through the baffles. The maximum velocity reaches 0.1 m/s whereas the minimum one is 0.

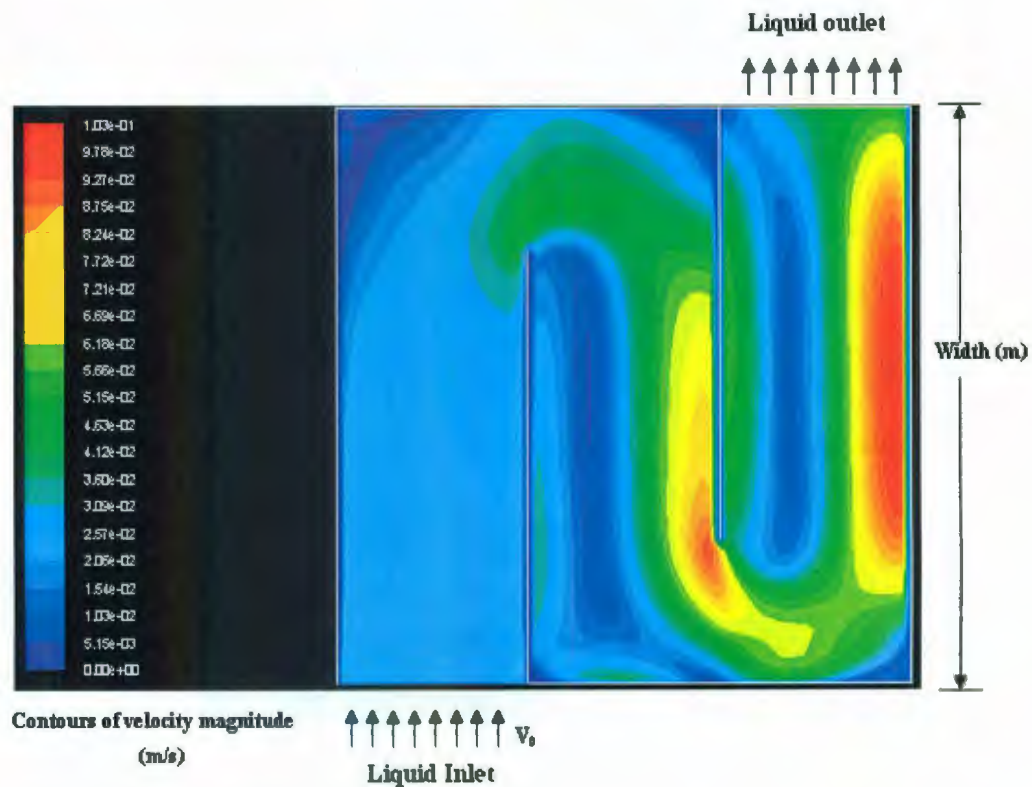


Figure A.2 Contours of liquid velocity magnitude in shell side from FLUENT 6.3



